Uɴɪᴠᴇʀsɪᴛʏ ᴏғ Zᴀɢʀᴇʙ

Fᴀᴄᴜʟᴛʏ ᴏғ ᴍᴇᴄʜᴀɴɪᴄᴀʟ ᴇɴɢɪɴᴇᴇʀɪɴɢ

ᴀɴᴅ ɴᴀᴠᴀʟ ᴀʀᴄʜɪᴛᴇᴄᴛᴜʀᴇ

Aᴇʀᴏɴᴀᴜᴛɪᴄᴀʟ ᴇɴɢɪɴᴇᴇʀɪɴɢ

FSB TX TEAM

Team Members		AIAA Number
Tibor Gašparac		922274
Matea Lišnić		922383
Hrvoje Magdić		922583
Antonio Golub		922306
Kristijan Ruklić		922275
Antonio Klasnić		922565
Vjekoslav Sraga		922397
Antonio Jurišić		922338
Fran Delić		922300
Ivan Kovačević		903859
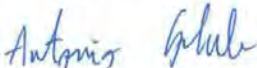
prof. dr. Pero Prebeg

prof. dr. Milan Vrdoljak

Contents

List of Figures

List of Tables

Nomenclature

A	A regression constant based on similar aircraft, [-]
A_{Roskam}	A regression constant [?], [-]
B	B regression constant based on similar aircraft, [-]
B_{Roskam}	B regression [?], [-]
k_f	weight reduction coefficient for fuselage, [-]
k_{lg}	weight reduction coefficient for landing gear, [-]
k_t	weight reduction coefficient for tail, [-]
k_w	weight reduction coefficient for wing, [-]
M_{ff}	total fuel fraction, [-]
W_E	empty weight of the aircraft, [lbs]
W_{crew}	weight of two pilots and their personal equipment, [lb]
W_{eq}	eqiupment weight, [lb]
W_{feq}	CLASS II fixed equipment weight, [lbs]
W_{PL}	payload weight, [lb]
W_{pwr}	CLASS II powerplant weight, [lbs]
W_{struct}	CLASS II structure weight, [lbs]
$W_{TO_{est}}$	estimated weight based on similar aricraft, [lbs]
A	Aspect Ratio, [-]
b_r	Wing span, [m]
C_D	Aircraft drag, [-]
C_{D0}	Aircarft drag with $C_L = 0$, [-]

$c_{L_{max}}$	Max lift coefficient , [-]
CGR	Climb gradient, [-]
CGR	climb gradient, [rad]
e	Oswald coefficient, [-]
h	Aircraft altitude, [m]
h	altitude, [m]
k_1	constant, [-]
k_2	constant, [-]
L/D	Lift to drag ratio, [-]
L/D	lift/drag ratio, [-]
n_{max}	Load Factor, [-]
n_{max}	Loading coefficient, [-]
P_{dl}	parameter, [-]
RC	Climb speed, [m/s]
S	Wing surface, [m^2]
$(\Lambda_{c/4})_T$	tail sweep angle, [°]
$(\Lambda_{c/4})_w$	wing sweep angle, [°]
$(\Lambda_{LE})_w$	wing leading edge, [°]
$(\Lambda_{TE})_w$	wing trailing edge, [°]
$(AR)_w$	wing aspect ratio, []
$(AR)_T$	tail aspect ratio, []
$(c_A)_T$	tail MAC, [m]

$(c_A)_w$	wing mean aerodinamic chord [MAC], [m]
$(c_t)_T$	tail tip chord, [m]
$(x_A)_T$	distance tail MAC, [m]
$(x_A)_w$	distance wing MAC, [m]
Γ_T	tail dihedral, [°]
Γ_w	wing dihedral, [°]
λ_T	tail taper, []
λ_w	wing taper, []
$\ni_s$	shock absorber efficiency, []
$\ni_t$	tire absorber efficiency, []
$\overline{X}_{ac}$	Aerodynamic center
$\overline{X}_{cg}$	Center of gravity
CG	center of gravity, []
d_s	diameter of shock absorber, [mm]
i_T	tail angle of incidence, [°]
i_w	wing angle of incidence, [°]
l_s	length of shock absorber, [mm]
$MTOW$	maximum takeoff weight, [kg]
N_g	load factor, []
P_M	static load on main gear, [kg]
P_N	static load on nosegear, [kg]
P_{Ndin}	dynamic load on nosegear, [kg]

s_s	stroke of the shock absorber, [mm]
S_{wet}	Aircraft surface, [m^2]
V_{Ffus}	fuselage fuel reservoir volume, [m^3]
V_{Freq}	required fuel reservoir volume, [m^3]
V_{Fwing}	wing fuel reservoir volume, [m^3]
W_F	required fuel weight, [kg]
w_t	touchdown rate, [fps]
W_L	landing weight, [kg]
W_{TO}	takeoff weight, [kg]
MAC	mean aerodynamic chord, [mm]
MAC	mean aerodynamic chord, [mm]
s_{FL}	Landing runway length, [m]
s_{TOG}	Take off runway length, [m]
T	Take off thrust, [kN]
T/W	Engine loading, [-]
T/W	thrust to weight ratio, [-]
V_A	Approach speed, [m/s]
V_A	approach speed, [m/s]
V_{cruise}	Cruise speed, [km/h]
V_n	Maneuvering speed, [m/s]
V_S	Stall speed, [m/s]
V_{SL}	stall speed, [m/s]

V_{TO}	Take off speed, [m/s]
W/S	Wing loading, [N/m^2]
q	Dinamic pressure, [N/m^2]
q	dynamic pressure, [N/m^2]
γ	Angle of climb, [°]
γ	flight path angle, [°]
Λ	Bypass-ratio, [-]
Λ	bypass-ratio, [-]
μ_g	Ground friction coefficinet
μ_g	friction coefficient, [-]
ρ	Air density, [kg/m^3]
ρ	air density, [kg/m^3]

1 Airplane configuration and mission analysis

1.1 Mission analysis

This airplane was made with respect to the mission given by the RFP, which can be divided into 16 phases shown on the diagram below (figure 1). Every number on the diagram represents one phase of the mission which will be discussed in detail later in the text.
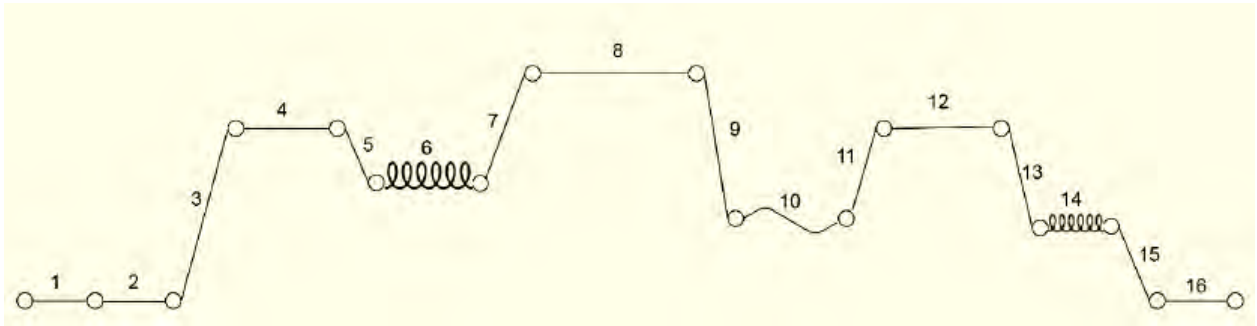
Figure 1: Mission

Mission phases given by the RFP (*Request for Proposal*):

1) Warm up and taxi

2) Take off

3) Climb from the sea level to the cruise altitude

4) Cruise ($150nm$ – BCA and BCM)

5) Tanker rendezvous at the altitude of 20000 ft at the speed of 300 KIAS

6) Air refueling simulation (20 minutes at the altitude of $20000ft$, $250KIAS$)

7) Climb from the altitude of 20000 ft to BCA (lowest fuel consumption regime)

8) Cruise at BCA with the BCM

9) Descent to the altitude of $15000ft$

10) 20 minutes long air combat and maneuvering training (max 8-9 g)

11) Climb to the BCA (lowest fuel consumption)

12) Cruise ($150NM$ BCM)

13) Descent on $10000ft$

14) Loiter at the altitude of 10000 ft with optimum endurance speed (30 minutes or 10% of total mission duration)

15) Descent to the sea level

16) Landing

For the purpose of weight estimation, it is necessary to mention that the aircraft will have no external fuel tanks ("clean configuration"). The mission described above was used to determine the airplanes which are meant to complete a similar mission, which gave us the information about possible configuration solutions. Threshold and desirable values of some performances were demanded by the RFP which will be shown in the table below, but since it isn't possible to maximize all of the performances, the final value of some airplane performance will depend on previously determined objectives with respect to their importance. AHP method was used to determine the level of importance of the objectives that were set earlier. Airplane performances demanded by the RFP.

Table 1: RFP requirements

Performance	Threshold value	Objective value
Maximum loading at $15000ft$	8	9
Ceiling	40000	50000
Runway length	8000	6000
Payload [lbs]	500	1000
Maximum range [NM] without refueling	1000	1500
Cruise speed [Ma]	0.7	0.8
Dash speed [Ma]	0.95	1.2

1.2 Aircraft configuration

1.2.1 Introduction

Based on the gatehered information about similar airplanes, shown earlier in the text, 3 possible jet fighter training aircraft configurations were designed. The purpose of this report is to describe the method which was used to choose the best of the 3 possible configurations taking in considerations all the pros and cons with respect to the objectives previously set. Furthermore, 2 additional configurations were taken into consideration, including 2 already built airplanes (Aermacci M-346 Master and Kai T-50) so it could be possible to conclude if there already is a better configuration of the 3 previously generated. The following text deals with the procedure used to determine the objectives and describes them more thorougly. Afterwards, the process of choosing the best and final configuration will be explained more thoroughly as well.

1.2.2 Discusing the factors which do have significant meaning to design

List of the objectives with significant meaning

Defining the main objectives is crucial for the progress of the project, so every next decision that follows the previous one can be consistent well argumented. After detailed jet trainer aircraft objective analysis it was decided that the main objectives of this project will be:

- life cycle cost minimization

- runway length minimization

- maximizing the overall maneuverability of the airplane

Explanation

- **Life cycle cost minimization** Jet fighter trainer airplanes are characterized by the large amount of operating hours, much more than any other type of airplanes. Due to that fact, this type of airplane requires more frequent maintenance operations. With the asumption that this airplane will serve no other than training purposes, it is decided that the main objective of this project should be the minimization of the life cycle cost because it has a large influence on the overall airplane cost. Life cycle cost includes the cost of design, manufacturing, operational costs (fuel consumption, periodic airplane modifications etc.), disposal costs and many more.

- **Runway length minimization** Take-off and landing phases are critical in every mission (civil or non-civil), due to the fact that they require a high level of engagement of the pilot compared to all other phases of the mission. By minimizing the runway length, the duration of those critical phases is reduced, which reliefs the pilot and reduces the need of infrastructural investments

- **Maximizing the overall maneuverability level** Aircraft's maneuverability level is defined with the ability to change it's attitude as fast as possible. Since the purpose of this project is design of the new 5th generation jet fighter training aircraft, it was decided that this airplane should have the highest possible maneuverability so it could reduce pilot's adjusting time, once he is done with the training process. The fact that the degree of maneuverability grows with the increase of forces and moments acting upon the control surfaces will be used later in the design process.

1.2.3 Multicriteria decision making

After all the objectives had been set, it was necessary to evaluate them so it could be possible to decide which of them are more important than the others and how much. By determining the main objective, the project can be continued in that way. The evaluation was done with by using the scale from 1 to 9 and comparing every objective with respect to two other objectives based on the average grade which was calculated from the evaluation given by every member of the team himself.
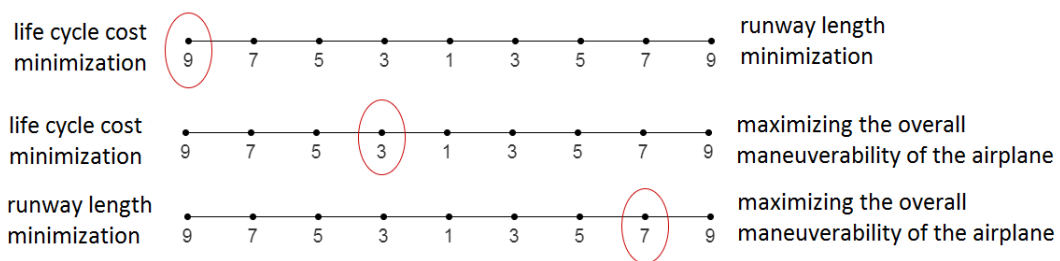
Figure 2: Multicriteria decision making

After evaluating the objectives, *AHP* method was used to determine which objective was most

important. All the calculations of the given method were made using the MATLAB software, which resulted with the following pie chart:
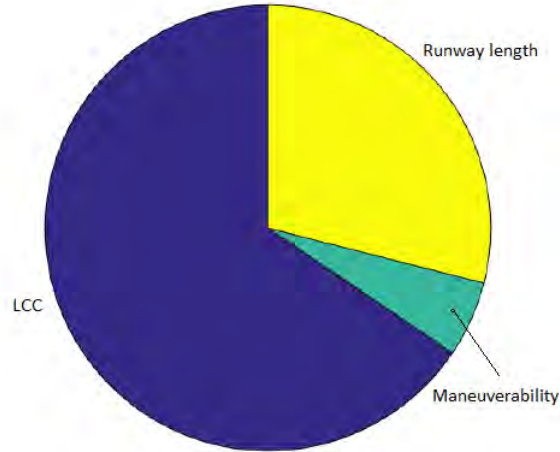
Figure 3: Objectives

1.2.4 General Aircraft Configuration

Based on similar aircraft and the given mission, it has been decided that only conventional configurations will be considered since they are cheapest and easiest to manufacture. Additional surfaces (eng. cannards) were rejected due to the additional drag that they produce. We will now examine the advantages and disadvantages from certain elements to determine the final configuration of the aircraft.

The following elements of the configuration will be examined:

- Wing type

- Wing position

- Stabilizing sufraces type

- Undercarrage type

1.2.5 Wing position

Table 2: Wing position

Low wing position	Mid wing position	HIgh wing position
+landing gear can be placed in wings +wing can float in water landings +continuous spar +easier access during maintenance +higher maneuverebility ----- -lower visibility -posibility of wing damage during ground operations	+least interferance drag +lower „groundeffect" that the low wing position +symmetrical flow around the aircraft +posibility of carying cargo outside +higher roll stability +higher flight speeds ----- -takes more fusselage volume -maintenance more difficult than a low wing position -increased landing gear length -non-continuos spar -higher mass of the hull frame	+higher engine clearance +lower chance of wing damage during ground operations +better cockpit visibility +better longitudinal stability ----- -maintenance more difficult -more robust landing gear

Table 3: Stability surfaces

Conventional tail	T-tail	Double tail
+Good stability and maneuverability with the smallest mass +most common type	+shorter vertical stabilizer due to the end plate effect +horizontal surfaces moved outside the wake flow ----- -heavier construction -access during maintenance more difficult -low efficiency at high angles of attack	+rudder moved from the central axis to not be in wake at high angles of attack +lower tail height ------ -heavier than the conventional construction

Landing gear configuration While considering the posible landing gear configurations, it has been decided that a conventional tricycle configuration will be used. Main landing gear struts can be placed in the hull ori n the wings. Placing the main landing gear in the wing means a higher lateral stability during take off and landing, but also longer struts. This in term decreases the stiffness of the construction meaning that the construction would need to be

heavier. Furthermore, this would reduce the available space in the wings for the fuel reservoirs. Finally, it has been decided that all the struts will be placed in the hull.

Engine location The RFP states that comertially available engines will be user since developing a new engine for a smaller aircraft series would not be economical. In order to decrease the Life Cycle Cost, one engines will be used. The best position to place the engines is the hull, with intakes positioned at the root of the wing.

Intake position

Nose

+ good intake flow without aircraft interferance

− Long intake, higher mass, high friction losses

Underhull

+ no flow interference at higher angles of attack, possibility of placing an engine in the nose

− Front leg placement, danger in foreign object damage, intake flow interference, intake needs to be 50 to 80% of the intake diameter above ground

Side of the hull

+ smaller hull dimensions from the above, no inlet interferance

− stability problem when inlets merge before the first stage of the compressor

Armpit

+ no foreign object damage during take off and landing, shorter inlet pipe, simplest construction enableing the wing to be directly joined to the hull, best position to minimize maintenance time (no need for ground equipment)

− Boundary layer interferance from hull and wings, sensitive to higher angles of attack and sideslip
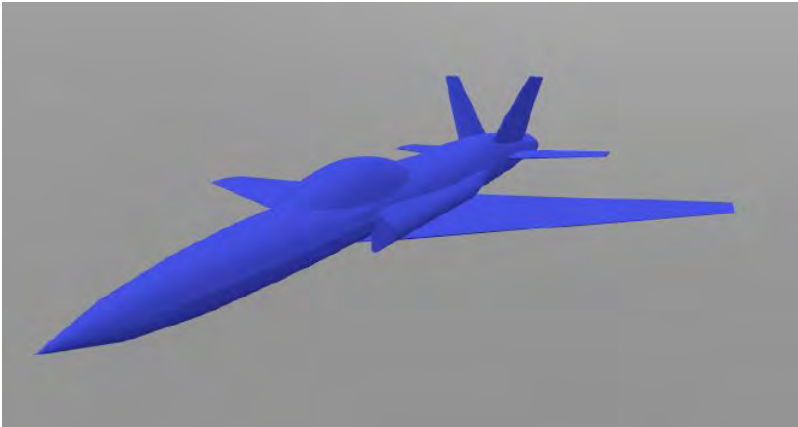
Figure 4: Configuration 1
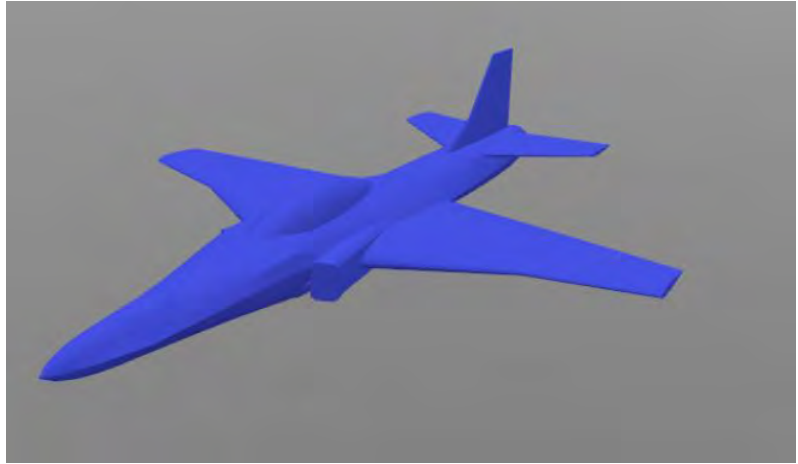
Figure 5: Configuration 2
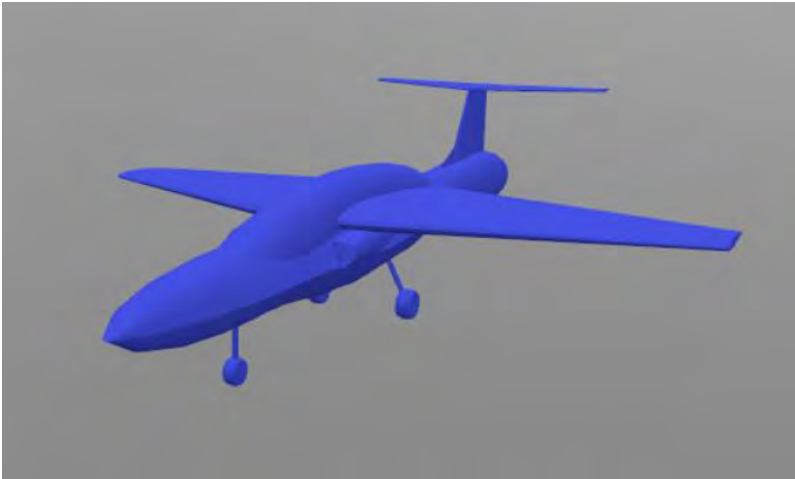
Figure 6: Configuration 3

Considered configurations Based on the above, three different configurations were made (shown on images 4, 5 and 6). Also, two additional aircraft were considered, Kai T-50 and M-346. Using the AHP method, the following priority vector diagram was calculated (figure 7)
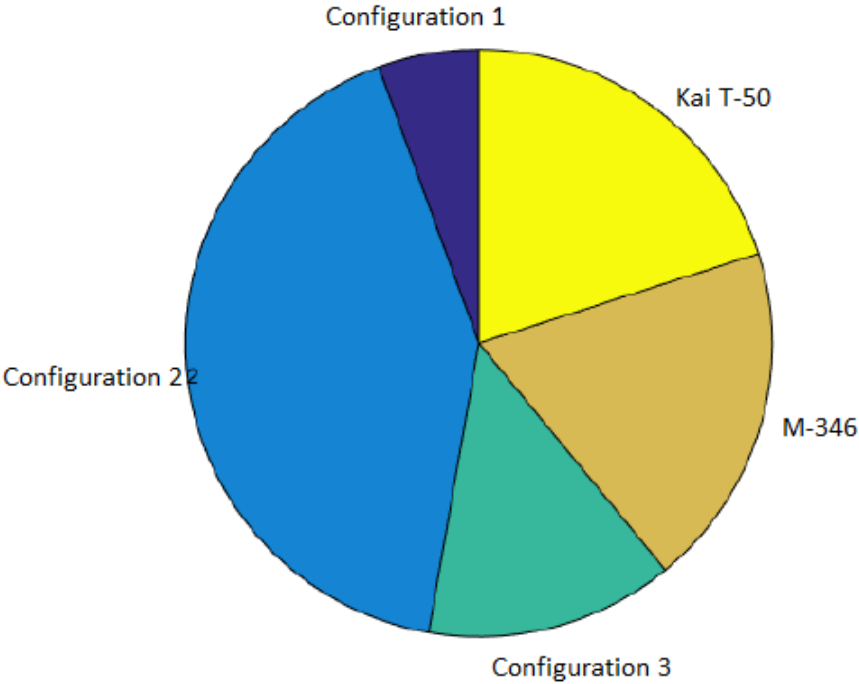
Figure 7: Priority vector diagram

As seen on figure 7, configuration 2 was selected as the best configuration for the previously determined objectives and will be further developed.

2 Weight estimation

This chapter shows weight estimation of military trainer described in previous chapters. RFP stated objectives and thresholds which have to be fulfilled. Regarding those reqirements, weight estimation was conducted as a trade study. Biggest issue at the begining of conceptual design of this aircraft was engine selection. After thorough research, five engines were selected (GE F404, GE F414, GE F110, Snecma M88 and Honeywell F125). Data for these five engines was aquired using Jane's Aero Engines [20] and for them was weight estimation conducted.

2.1 Class I

Class I weight sizing was completed following iterative process as described in [1]. Fuel weight was determined using fuel fractions in every phase of mission. After calculating fuel fractions and fuel weight, empty weight was determined. Maximum takeoff weight was calculated as a sum of all component weights. In summary, that was class I weight estimation and more detailed estimation process follows.

According to [1], regression constants had to be determined using similar aircraft. These constants are iportant for empty weight calculation. In [1], regression constants for military trainer were

$$A_{Roskam} = 0.6632$$

$$B_{Roskam} = 0.8640$$

(1)

Using data of similar aircraft, which are shown in table 4.

Table 4: Similar aircraft

Aircraft	W_{TO} [lbs]	W_E [lbs]
T-38 Talon	12092	7209
T-45 Goshawk	13393	9394
Hongdu L-15 Falcon	14330	9921
Alpha jet	15432	7661
Hawk T2	20062	10935

Because of time that has passed since Roskam Part 1 [1] was released, for similar aircraft were

chosen aircraft that don't have large amount of composite and other newer and lighter materials. That has been done so that process described in [1] can be applied to this project.

As it was previously stated, weight estimation is iterative process and $W_{est} = 15432$ lbs was weight chosen for a beginning of iterative process. In figure 8 are shown regression curves based on [1] and on similar aircraft, takeoff and empty weights of similar aircraft and beginning weight estimation of iterative process.
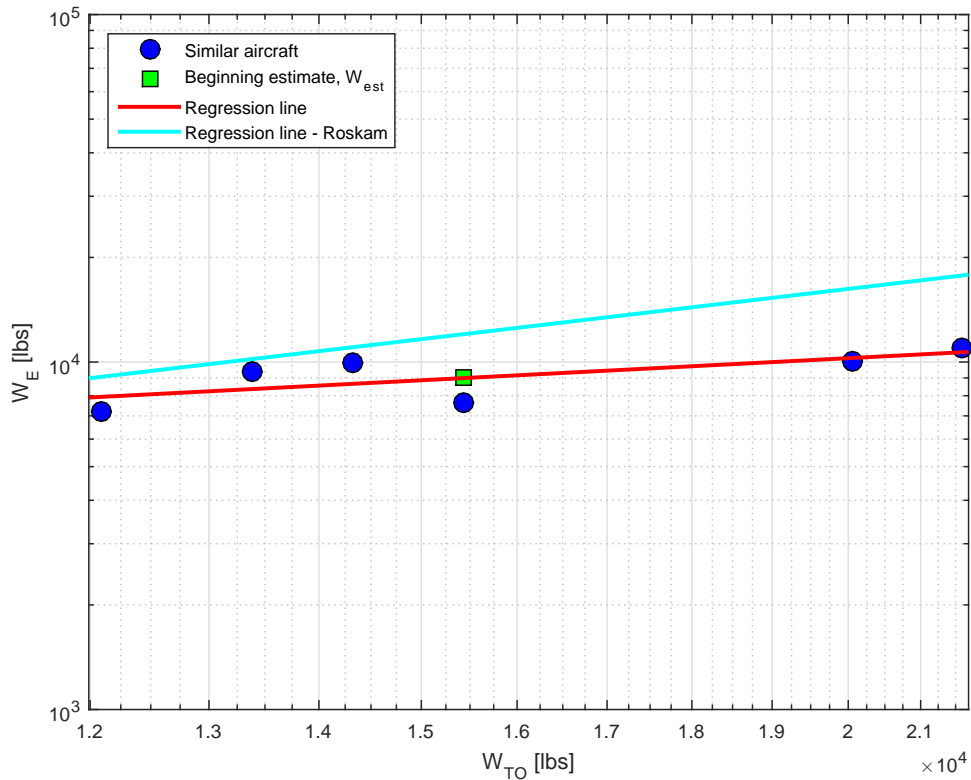
Figure 8: Regression

Regression constants are last of all information that had to be aquired based on similar aircraft. Having all neccessary data, fuel fractions can be calculated using equation

$$M_{ff} = \frac{W_1}{W_{TO}} \prod_{i=1}^{16} \frac{W_{i+1}}{W_i} \qquad (2)$$

Fuel fraction for air combat mission phase was calculated as described in Aircraft Design: A Conceptual Approach [19] because [1] haven't provided ways to calculate this particular mission phase. After fuel weight, empty weight can be estimated. Using regression constants, linear

dependance of empty weight and takeoff weight is used

$$W_E = 10^{\frac{logW_{TO}-A}{B}} \tag{3}$$

However, lighter materials (composites, etc.) are supposed to be used so weight reduction coefficients are introduced

$$k_w = 0.75; \quad k_t = 0.75; \quad k_f = 0.85; \quad k_{lg} = 0.88, \tag{4}$$

where k_w is weight reduction coefficient for wing, k_t for tail, k_f for fuselage and k_lg for landing gear.

Including weights given in RFP [18]

$$W_{eq} = 1345 \, \text{lb}$$
$$W_{crew} = 550 \, \text{lb} \tag{5}$$
$$W_{PL} = 500 \, \text{lb}$$

results of weight estimation are shown in table 5

Table 5: *Trade study* analisys

Engine	$\mathbf{W_{TO}}$ [lbs]	$\mathbf{W_E}$ [lbs]	$\mathbf{W_F}$ [lbs]	$\mathbf{(T/W)_{TO}}$	Diameter [in]	Length [in]
F404	11233	7787	2948	1.5806	34.65	158.66
F414	11233	7787	2948	1.9579	34.65	158.66
F110	13292	7800	4405	2.1811	46.46	181.89
Snecma M88	10911	7075	2729	1.5448	27.56	139.37
Honeywell F125	11023	7110	2802	0.8239	35.98	124.02

2.2 Class II

Class II weight sizing was completed following process as described in Roskam Part V [5]. Weight of each component of aircraft was calculated and empty weight is given as a sum of all component weights. It should be noted that Honeywell F125 engine was chosen as a power unit which will be described in detail in following chapters. Table 6 shows component weights of aircraft.

Table 6: Component weights

Component	Weight [lbs]
W_{struct}	3463.1
W_{pwr}	1854.5
W_{feq}	2010.1

By adding all the component weights, class II empty weight of aircraft is calculated and it is

$$W_E = 7327.6 \, \text{lbs} \tag{6}$$

In equation above is shown that class II weight estimation deviates less that 5% which means that class II weight is acceptable.

3 Performance estimation

3.1 Estimating wing area, take-off thrust and maximum lift coefficient

In order to meet the performance requirements defined in RFP, an estimation of wing area S, take-off thrust T, maximum lift coefficient for clean, take-off and landing configuration c_{Lmax} as much as aspect ratio A, is given in this chapter. The method has resulted in the determination of a range of values of Wing Loading W/S, Thrust loading T/W, and maximum lift coefficient C_{Lmax}, within which certain requirements are met. All set requirements and final solution were shown in matching diagram.

3.1.1 Take-off requirements

Take-off and landing requirements are defined in RFP, and it includes adding take-off and landing distance together for single engine aircraft. Besides that, these procedures are taken on icy runway with maximum gross weight.

The take-off groundrun may be estimated from:

$$s_{TOG} = \frac{k_1 \cdot (W/S)_{TO}}{\rho \cdot [C_{Lmax}(k_2 \cdot (X/W)_{TO} - \mu_g) - 0.72 C_{D0}]}, \tag{7}$$

with no wind and leveled runway. According to the requirements of the RFP, the aim is to minimize the runway length so we decided that the runway length s_{TOG} should be 457.2 m (1500 ft). Estimating is done for the standard day, with the runway friction coefficient μ_G=0.015 and lift coefficient c_{Lmax}=1.4 in take-off configuration. The parameter k_1 is 0.047 for jet engine, with the estimated bypass ratio of 0.35, so the parameter k_2 is

$$k_2 = 0.75(\frac{5 + \Lambda}{4 + \Lambda}) = 0.9224. \tag{8}$$

To determine the take-off conditions, the relationship between Thrust-to-Weight ratio and the Wing Loading determines the formula

$$(T/W) = \frac{\dfrac{k_1(W/S)}{s_{TOG} \cdot \rho} + 0.72 C_{D0} + \mu_g C_{Lmax}}{C_{Lmax} k_2}. \tag{9}$$

3.1.2 Landing requirements

Landing requirements for military aircraft are treated according to FAR 25 standard as well as for civil aircraft above 5700 kg. To met these requirements, we have decided to minimize the runway length, which is 6000 ft according to the RFP, and represents the runway length for take-off and landing procedure. Estimated lift coefficient in landing configuration is $c_{Lmax}=1.6$. Approach speed for FAR 25 standard is

$$V_A = \sqrt{\frac{s_{FL}}{0.3}} = 67.617 \ m/s. \tag{10}$$

Aircraft stall speed is

$$V_{SL} = \frac{V_A}{1.2} = 56.3475 \ m/s. \tag{11}$$

And at the end, values that determine the landing parameters depend on the Wing Loading according to the formula

$$(W/S) = \frac{V_{SL}^2}{2}\rho C_{LmaxL}. \tag{12}$$

3.1.3 Cruise requirements

The cruising speed is defined in the RFP specification. Since we have decided to minimize costs, as we have already said, which is the opposite of maximizing cruising speed, we will take a lower speed limit that meets the specification, and that is $Ma_{cruise}=0.7$. At cruising speed and altitude of 10058 m (33000 ft), with clear aircraft configuration and $(W_5/W_{TO})=0.9432$, Thrust-to-Weight ratio depends on the Wing Loading according to the formula

$$(T/W)_n = \frac{q_{combat}C_{D0}}{W_S} + \frac{W_S n_{max}^2}{q_{combat}\pi \ Ae_{clean}}0.875. \tag{13}$$

3.1.4 Maneuvering requirements

According to the requirements in the specification, it was decided to minimize the load factor due to low cycle cost, so the load factor will be $n_{max}=8$. Maneuvering is carried out at altitude of 4572 m (15000 ft) with a 50% of internal fuel capacity. With that amount of fuel, weight

ratio is (W_{11}/W_{TO})=0.875. This requirements are determined for the standard day and clean configuration. Thrust-to-Weight ratio is

$$(T/W)_n = \frac{n_{max}C_{D0}}{C_{Lmax}} + \frac{n_{max}C_{Lmax}}{\pi Ae_{clean}}. \tag{14}$$

3.1.5 Ceiling requirements

Operational ceiling for military trainer aircraft, is defined as an altitude at which it is still possible to achieve positive Rate of Climb of 0.5 m/s (100 ft/min). Limit of the 12192 m (40000 ft) was chosen to reduce the structure load and cost of structure lifespan. Lift to Drag ratio is

$$(L/D)_{maxceiling} = \frac{1}{2}\sqrt{\frac{\pi \cdot A \cdot e_{clean}}{C_{D0clean}}} = 11.147. \tag{15}$$

Thrust to weight ratio with the weight ratio (W_4/W_{TO})=0.9509, is

$$(T/W)_{ceiling} = \frac{RC}{\sqrt{\dfrac{2}{\rho\sqrt{\dfrac{C_{D0}}{\pi Ae_{clean}}}}0.9509(W/S)}} + \frac{1}{(L/D)_{maxceiling}}. \tag{16}$$

3.1.6 Engine

After reviewing all commercially available engines, the Honeywell F125IN engine was selected. Since the minimum required Thrust-to-Weight ratio is 0.8236, for the intended mass of 5000 kg, engine provides enough force to meet all these requirements. Other engines that were reviewed, provide more thrust than this one, but they were not chosen due to higher lifecycle cost of an aircraft with higher thrust to weight ratio. The technical data of chosen engine is given in the Table 7.

Table 7: F125IN Technical Data

Take-off thrust (Dry), N	25617
Take-off thrust (maximum afterburner), N	40383
Diameter, mm	914
Length, mm	3150
Weight, kg	618.5
Specific fuel consumption, mg/Ns	22
Cost, m$	2,5

3.2 Trade study

In this Trade Study influence of lift coefficient on performance is analyzed. All of the following diagrams were considered while deciding about appropriate performance point.

3.2.1 Lift coefficient influence on Take-Off

Diagram shows Thrust-to-Weight ratio vs. Wing Loading, for fixed take off distance and for various lift coefficients. For example, for take-off lift coefficient of C_L=0.9, acceptable are all combinations above the blue line. It is concluded that with lift coefficient increase, required thrust decreases while wing loading increases. Wing loading increase means decrease in wing area. Wide span of this lines with C_L=constant means more acceptable points. Regarding to project goals, chosen lift coefficient value will be as low as possible with limits on thrust and runway length.
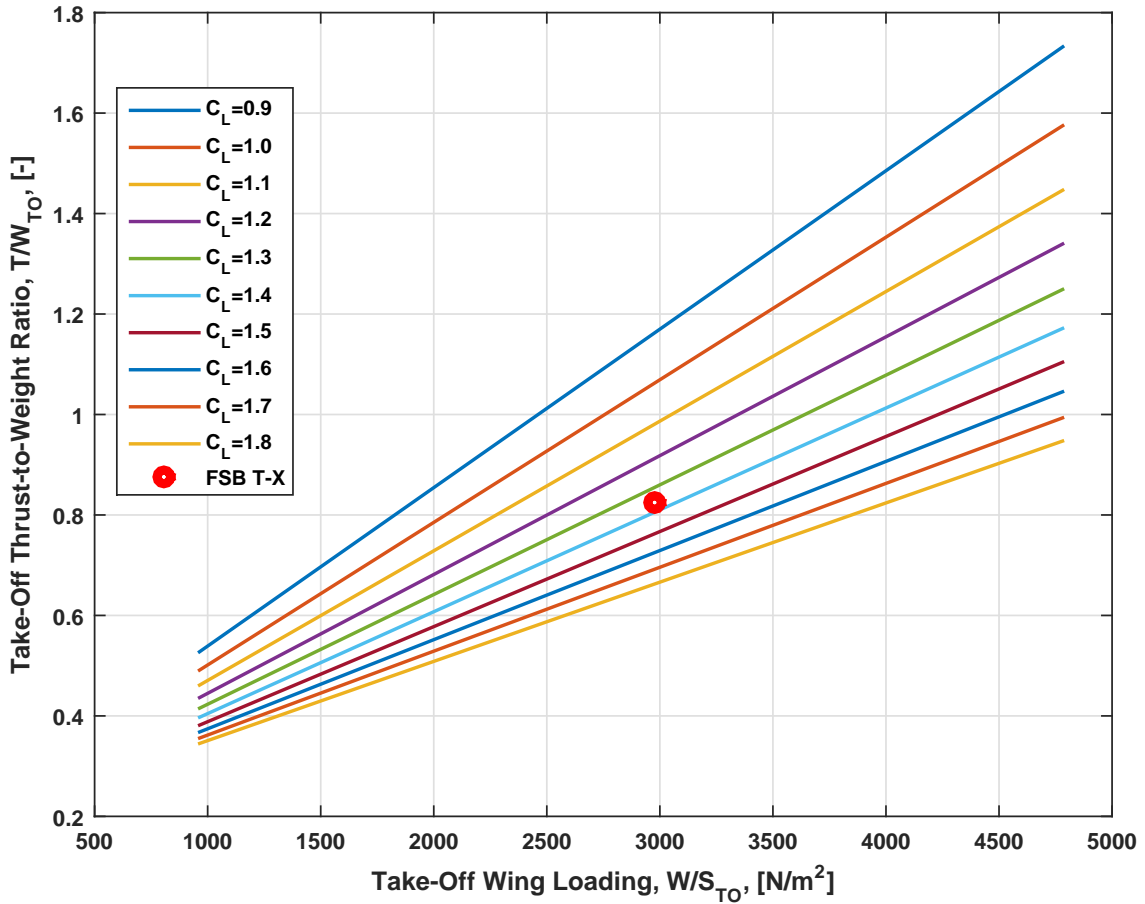
Figure 9: Lift coefficient with take-off requirements, A=5

3.2.2 Lift coefficient influence on landing conditions

Figure 10 shows relation of Thrust-to-Weight Ratio and Wing Loading, with regards to landing conditions. Diagram shows that with lift coefficient increase, needed wing area decreases, i.e. wing loading increases. Although greater Wing Loading is desirable regarding to Life Cycle Cost, Wing Loading is primarily limited by take-off demands on the other hand. With Wing Loading increase, Thrust-to-Weight ratio also increases which is negative consequence because, in general, more powerful engine means higher purchase price and higher maintenance costs.

Figure 10: Lift coefficient with landing requirements, A=5

Figure 10 shows relation of Thrust-to-Weight Ratio and Wing Loading, with regards to landing conditions. Diagram shows that with lift coefficient increase, needed wing area decreases, i.e. wing loading increases. Although greater Wing Loading is desirable regarding to Life Cycle Cost, Wing Loading is primarily limited by take-off demands on the other hand. With Wing Loading increase, Thrust-to-Weight ratio also increases which is negative consequence because, in general, more powerful engine means higher purchase price and higher maintenance costs.
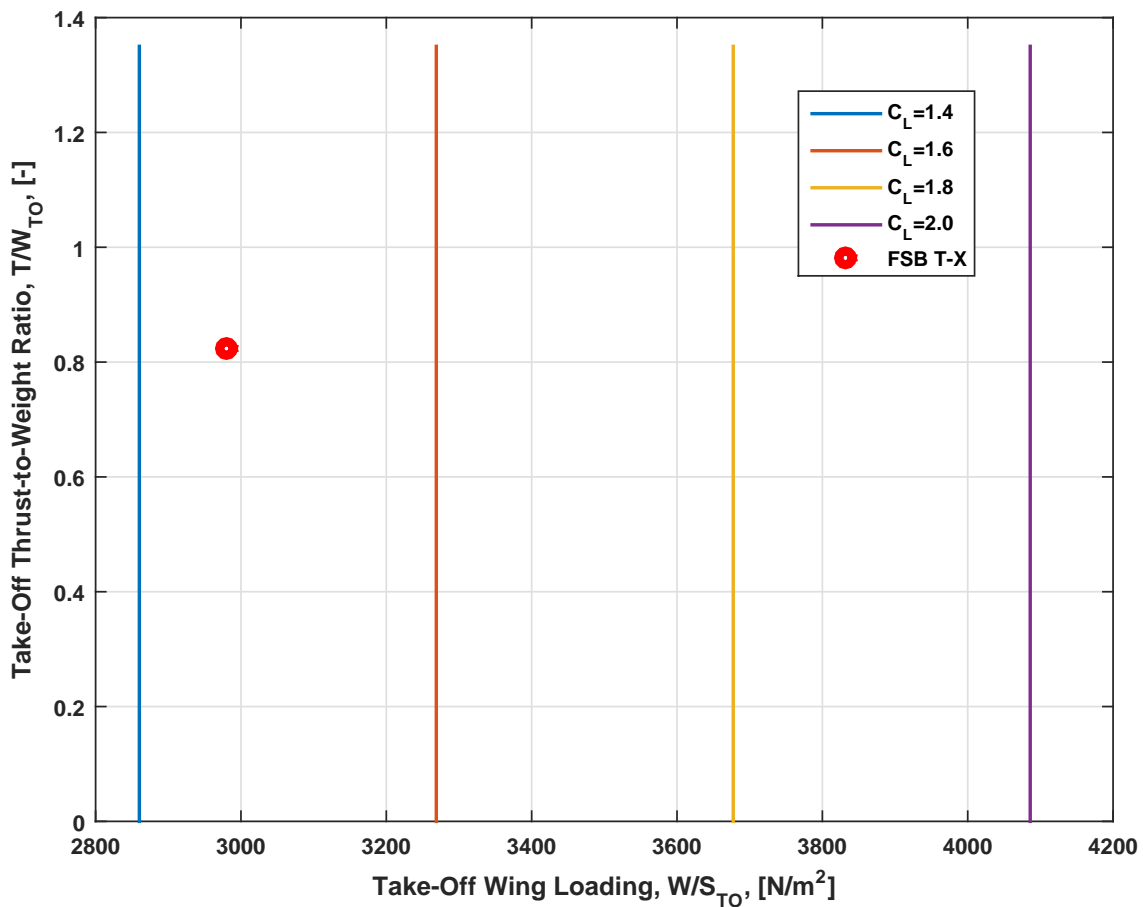
3.2.3 Lift coefficient influence on maneuvering

When considering maneuvering conditions, crucial variable is the load factor n. Figure 11 shows the diagram where Thrust-to-Weight ratio and Wing Loading increase with load factor increase. In RFP, minimum acceptable load factor is $n=8$. Curve with that load factor value is upper red curve. Because of RFP threshold, all values below that curve are not acceptable. That

means that maneuvering requirements are excluding conditions and need to be fulfilled. Range between of Wing Loading between 1000 and 1500 N/m^2 is interesting because of minimum values of Thrust-to-Weight ratio. Although is minimizing the Thrust-to-Weight ratio positive, that low Wing Loading means relatively large, i.e. expensive wing.
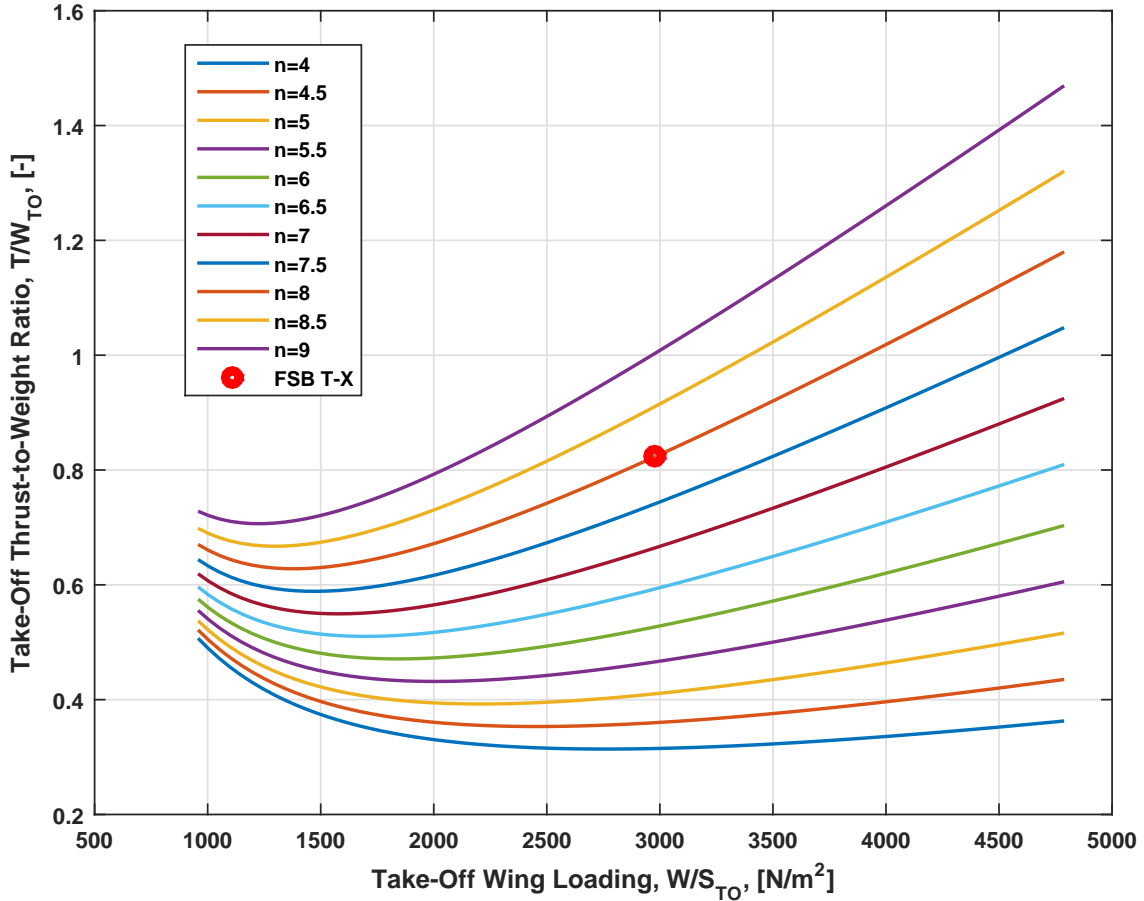
Figure 11: Lift coefficient with maneuvering requirements, A=5

3.3 Matching diagram with all limitations

After calculation of initial values, range of Wing Loading and Thrust-to-Weight ratio is assumed. Assumed range of Wing Loading is between 957 to 4788 N/m^2 (20 to 100 psf). That range was used to compute how Thrust-to-Weight ration depends on Wing Loading in maneuver. That dependence is displayed on matching diagram with purple color (figure 12).
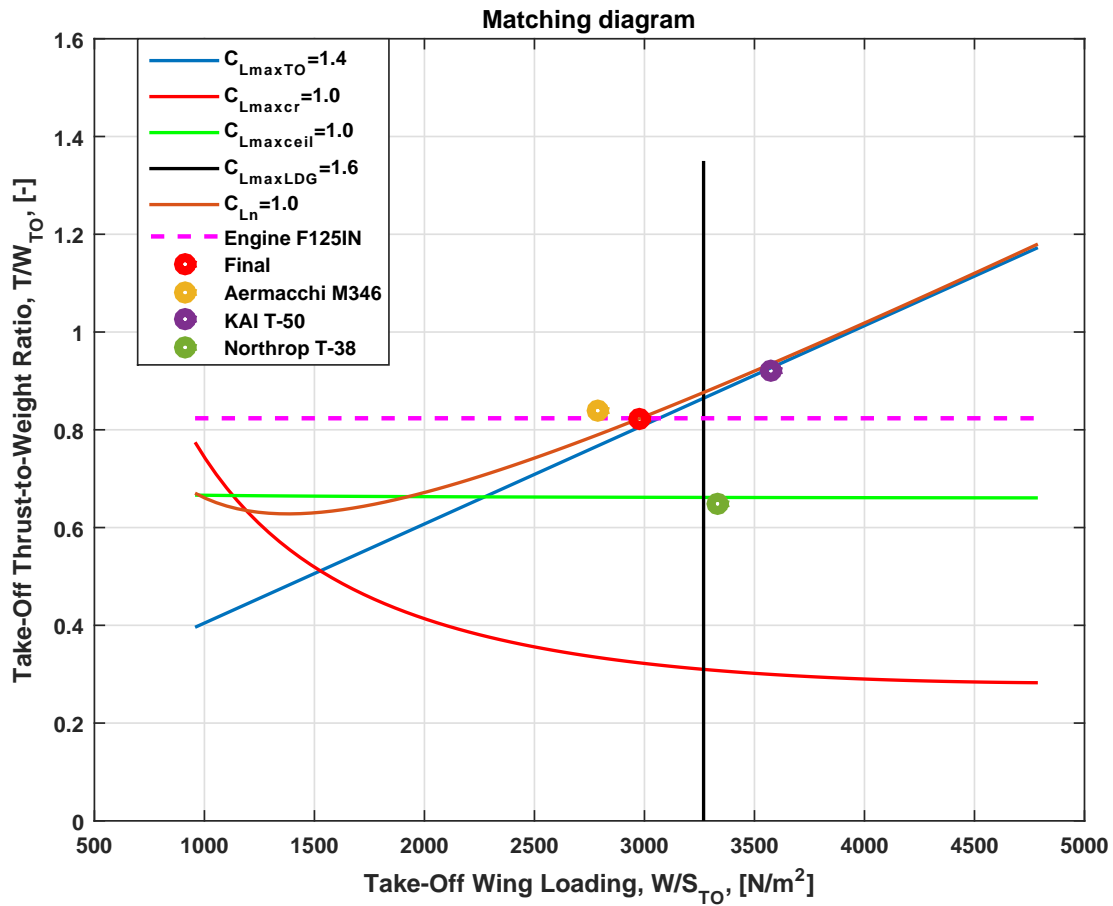
Figure 12: Matching diagram

Behavior of cruise parameters is shown with red curve, while ceiling parameters are shown with green line. For take-off requirements, range of Thrust-to-Weight ratio is assumed and Wing Loading is calculated. That dependence is illustrated with blue color in the matching diagram. Matching diagram also shows the maximum values of Wing Loading during landing, which decreases with shorter runway. That characteristic is illustrated black. Dashed pink line is Thrust-to-Weight with maximum engine thrust. Orange, blue and green points are Thrust-to-Weight ratios and Wing Loadings of similar aircraft. Characteristic point, i.e. Thrust-to-Weight ratio and Wing Loading for this aircraft is selected iteratively. On first iteration of matching diagram, few available of-the-shelf engines with enough performance are selected and drawn to matching diagram. Because of great load factor in maneuvering and according to trade study, demand on minimum load factor n=8 is also drawn to diagram. After that, full thrust characteristic of Honeywell F125IN was added to diagram. Experimenting with combinations of

lift coefficients during take off and landing, as seen in trade study, C_L for take off is reduced to C_L=1.4 for which the curve occurs nearly parallel to curve with constant n=8. With that data, lift coefficient for landing is minimized (vertical line). In the end, other non-critical curves are added to check all of the given flight requirements.

4 Wing and tail geometry

A trapezoid wing with a sweep of 30° (at 1/4 of the chord) was selected. A high sweep angle is suitable for high subsonic speeds because it increases the value of the critical Mach number. Unfortunately, a high sweep angle reduces the lift at lower speeds increasing the landing speed and landing/take off distance. A variable sweep wing was considered, but ultimately rejected because it would result in an increase in mass, maintenance complexity and *Life cycle cost.*

A mid wing configuration was selected as it provides the lowest interference drag and good longitudinal stability. Cabin visibility is also excellent which is important for trainer aircraft.

Aspect ratio $(AR)_w = 5$ was selected as it is a compromise between a low aspect ratio wing, with a high roll rate and simple construction and a high aspect ratio wing, with a lower interference drag.

The selected taper $\lambda_w = 0.33$ reduces the mass of the wing and gives a better wing load, making the construction of the wing simpler. Furthermore, it provides better performance when approaching stalling conditions.

A dihedral angle positively affects longitudinal stability, but since a feedback loop will be implemented the dihedral angle $\Gamma = 0°$ is selected to simplify the construction and manufacturing, reducing the mass and *Life cycle cost.* Table 8 shows the specifications and dimensions of the selected wing.

A standard configuration tail with an "All-Moving" horizontal tail was selected because of high subsonic speeds. This configuration reduces the mass and maintenance complexity of the horizontal stabilizer. The dihedral angles of the "All-Moving" horizontal tail is $\Gamma_{HT} = 0°$ to simplify the construction. The vertical stabilizer is a standard configuration with a rudder. Table 9 shows the specifications and dimensions of the selected tail.

Table 8: Wing parameters and dimensions

Parameter	SI	US
$(S)_w$	16.5 m^2	177 ft^2
$(b)_w$	9.08 m	29.80 ft
$(c_r)_w$	2.73 m	8.96 ft
$(c_t)_w$	0.90 m	2.96 ft
$(c_A)_w$	1.97 m	6.46 ft
$(x_A)_w$	1.28 m	4.20 ft
$(AR)_w$	5	
i_w	0 °	
Γ_w	0 °	
λ_w	0.33	
$(\Lambda_{c/4})_w$	30 °	
$(\Lambda_{LE})_w$	34.14 °	
$(\Lambda_{TE})_w$	15.38 °	

Table 9: Tail parameters and dimensions

	Horizontal stabilizer		Vertical stabilizer	
	SI	**US**	**SI**	**US**
$(S)_T$	3.724 m^2	40.085 ft^2	1.95 m^2	20.99 ft^2
$(b)_T$	3.860 m	12.664 ft	1.899 m	6.234 ft
$(c_r)_T$	1.287 m	4.222 ft	1.467 m	4.813 ft
$(c_t)_T$	0.643 m	2.110 ft	0.587 m	1.926 ft
$(c_A)_T$	1.000 m	3.280 ft	1.09 m	3.576 ft
$(x_A)_T$	0.567 m	1.860 ft	0.436 m	1.430 ft
$(AR)_T$	4		1.85	
i_T	0°		0°	
Γ_T	0°		90°	
λ_T	0.5		0.4	
$(\Lambda_{c/4})_T$	30°		40°	

4.1 Airfoil

Special attention was given when selecting the airfoil due to the contradictory goals of the aircraft. A short landing/take off distance requires an thicker airfoil with higher lift, while a high subsonic dash speed is easier to accomplish with a thinner airfoil with less drag. Furhermore, a thinner airfil has less mass but cannot hold the required fuel for the specified mission. After calculating the required section lift, a trade study was made with 3 NACA 6-series airfoils to determine the best one. Figure 14 shows the section lift calculated with XFLR5 at different angles of attack. NACA 63209[12] was selected as it provides enough lift and space for fuel with a low thickness of 9%. Experimental data for NACA 63209 is available[27] and shown in figure 14. Experimental and numerical data match well on smaller angles of attack while there is a significant difference at angles closer to stall. Figure 13 shows the selected NACA 63209 airfoil with 200 panels. The thinner airfoil, NACA 64008 does not provide enought section lift. Also, it would not provide enough space for the fuel tanks. On the other hand, the thicker airfoil provide enough lift but the large thickness increases drag and the weight of the wing.
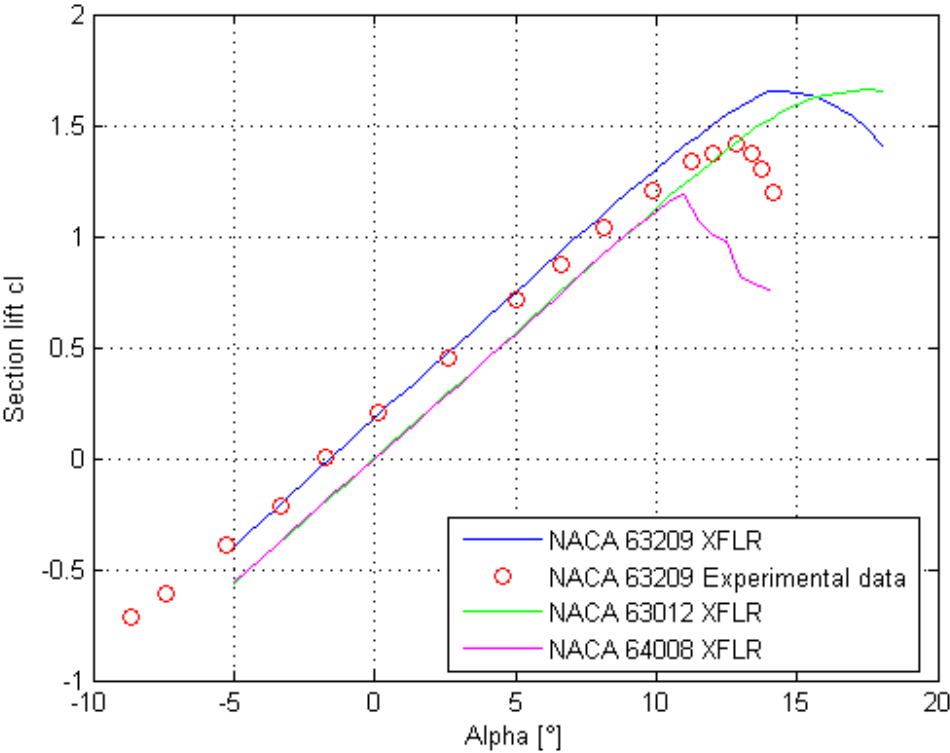
Figure 13: NACA 63209 with 200 panels

Figure 14: Comparison of section lift for different NACA 6-series airfoils

For the tail surfaces, the symmetrical and well documented NACA 0009 was selected (figure 15).

Figure 15: NACA 0009 airfoil

4.2   Additional lift surfaces

Additional lift surfaces are required to accomplist the required lift for taking off and landing. In order to reduce mass and LCC, plain flaps with no slats will be implemented. Three positions are available, 0° for flight, 20° for taking off and 40° for landing (figure 16). Additional lift was calculated from analitical formulas [1] and checked using XFLR5 (figure 17).
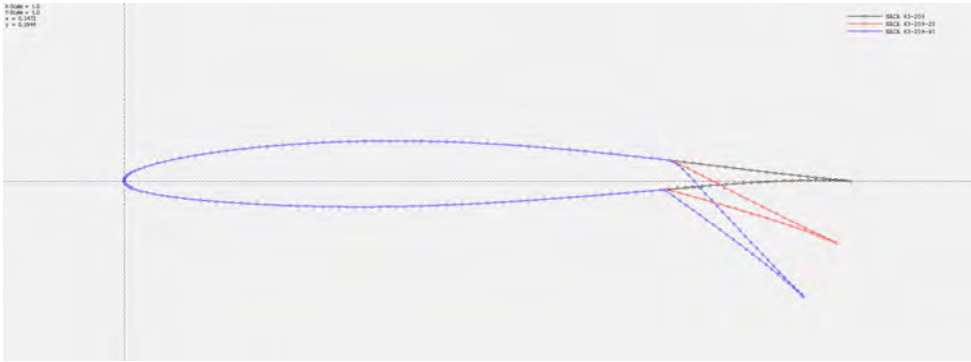

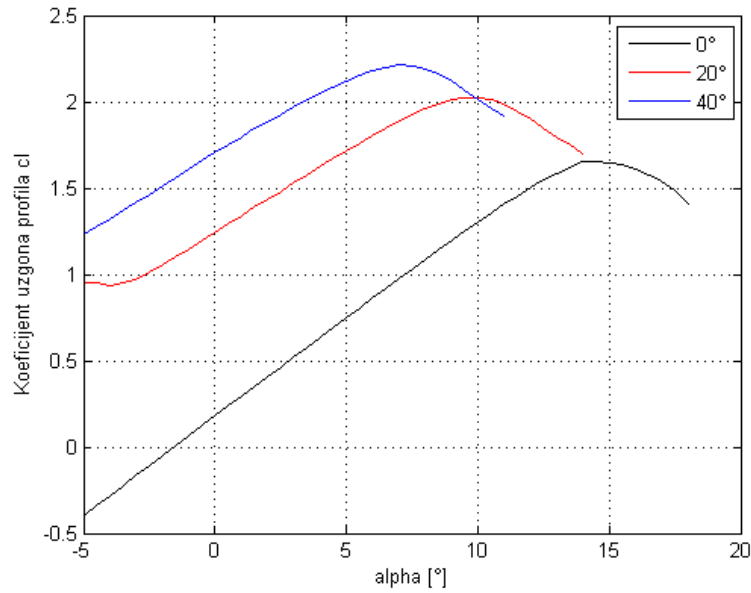Figure 16: NACA 63209 with different flaps settings

Figure 17: Section lift increase for different flaps settings

The flaps are positioned on the last 1/4 of the chord length ($c_f/c = 0.25$) from the root to 60% of the span of the wing. Ailerons are positioned on the last 1/4 of the chord length and span from 60% to 90% of the wing span. The rudder is also positioned on the last 1/4 of the chord of the vertical stabilizer as spans from the root to 90% of the height of the vertical stabilizer.

4.3 Fuel reservoirs

An estimated fuel mass for the mission is $W_F = 1271\,kg$, meaning a required minimum reservoir of $V_{Freq} = 1.588\,m^3$. The fuel reservoires are located between the front and back spar and an analitical estimate [1] gives an reservoir volume of $1.12\,m^2$. A CAD model (figure 18) of the conceptual wing was made to confirm the reservoir volume.

Finally, it was decided that the wing reservoirs will hold $V_{Fwing} = 1.1\,m^3$, while an additional reservoir $V_{Ffus} = 0.5\,m^3$ will be placed in the fuselage.
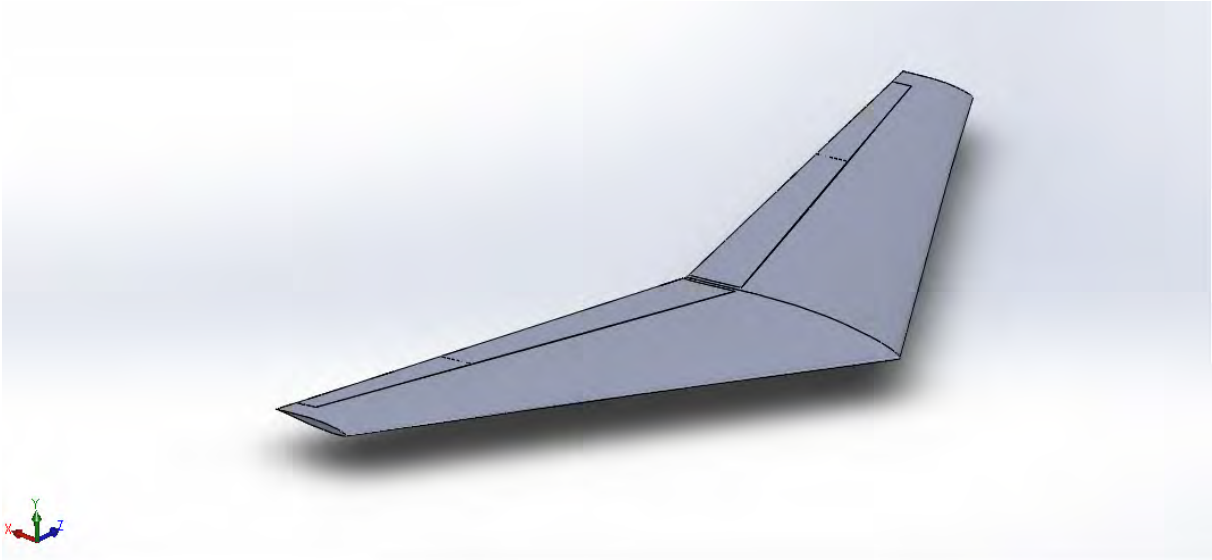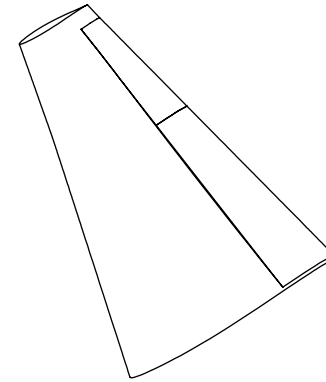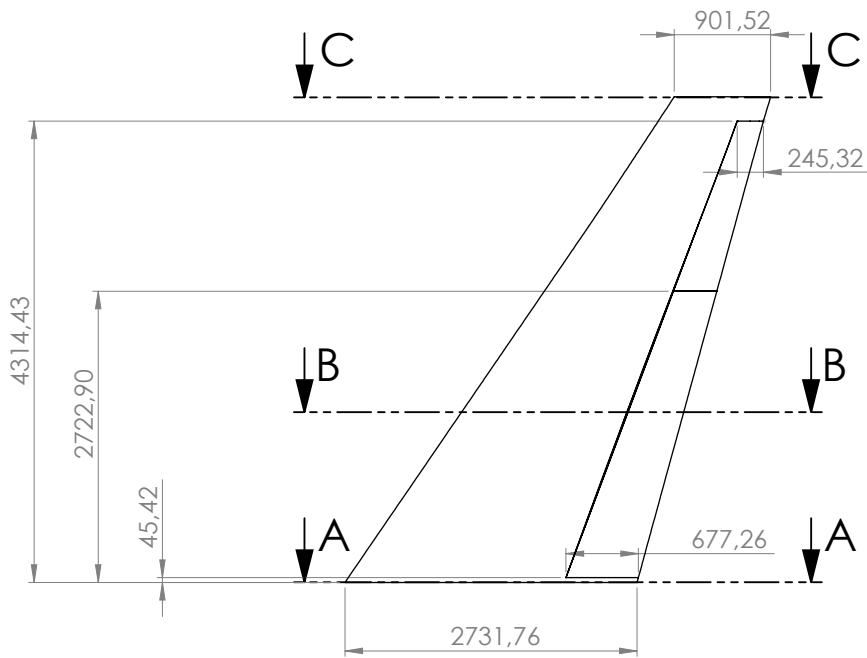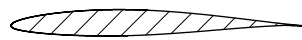
Figure 18: Wing model in SolidWorks

4541,50

901,52

245,32

C   C

4314,43

2722,90

B   B

45,42

677,26

A   A

2731,76

SECTION A-A

SECTION B-B

SECTION C-C

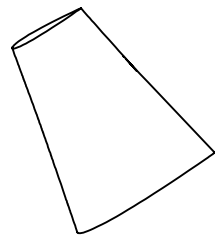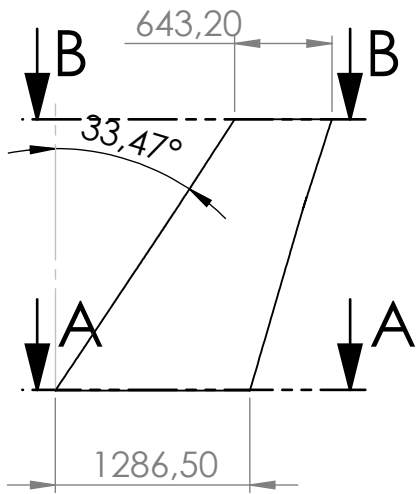|	NAME	SIGNATURE	DATE			TITLE:	
DRAWN							
CHK'D							
APPV'D						**FSB TX Team**	
MFG							
Q.A			MATERIAL:		DWG NO.		A3
						WING	

UNLESS OTHERWISE SPECIFIED:
DIMENSIONS ARE IN MILLIMETERS
SURFACE FINISH:
TOLERANCES:
   LINEAR:
   ANGULAR:

FINISH:

DEBURR AND
BREAK SHARP
EDGES

DO NOT SCALE DRAWING   REVISION

WEIGHT: SCALE:1:50   SHEET 1 OF 1

1794,70

643,20

33,47°

B B

A A

1286,50

SECTION A-A

SECTION B-B

	NAME	SIGNATURE	DATE			TITLE:	
DRAWN						**FSB TX Team**	
CHK'D							
APPV'D							
MFG							
Q.A			MATERIAL:		DWG NO.	Horizontal stabilizer	A4
			WEIGHT:		SCALE:1:50		SHEET 1 OF 1

587

158,89

B

B

D

D

43,68°

1899

1709,10

A

A

C

C

362,99

1467

B

B

SECTION A-A

SECTION B-B

	NAME	SIGNATURE	DATE			TITLE:	
DRAWN						FSB TX Team	
CHK'D							
APPV'D							
MFG							
Q.A				MATERIAL:		DWG NO.	A4
						Vertical stabilizer	
				WEIGHT:		SCALE:1:20	SHEET 1 OF 1

A

A

5 Undercarriage design

Undercarriage is essential aircraft component, for the following functions: support the aircraft when in place or towed, taxi and steer on the ground using an aircraft's own power, the take off run and landing and braking on the runway. Most commercial and training airplanes have nose undercarriage ("tricycle type"), that is some kind of standard for that type of aircraft, consequently in this project was taken a retractable tricycle configuration (figure 19). The gears were chosen to be retractable in order to decrease drag on the aircraft.

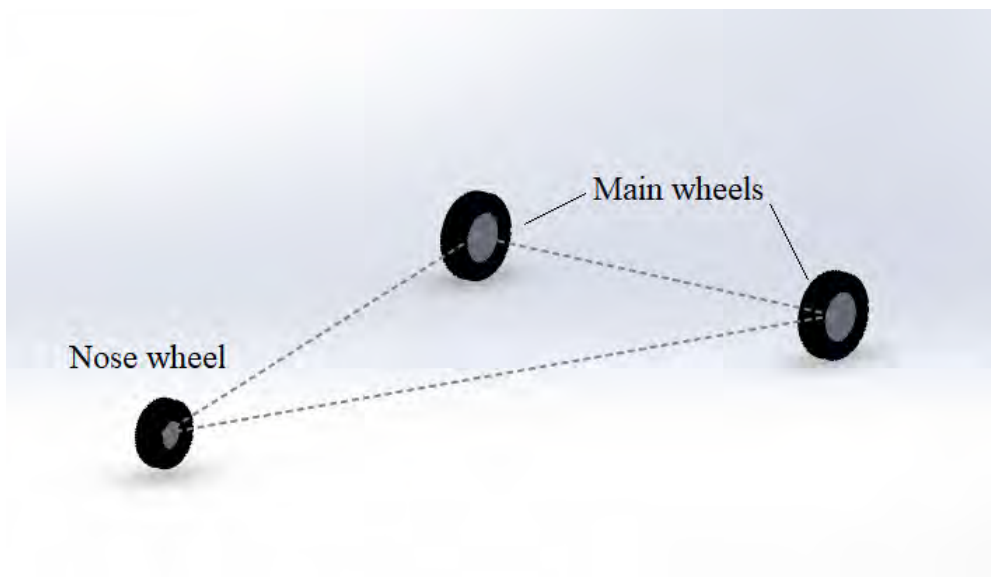Figure 19: Tricycle configuration

Advantage of tricycle undercarriage:

- View over the nose is excellent

- Faster and straighter at taxing

- Move comfortable when boarding

- Better ground stability, less ground loop and permits full

- Small wing incidence, permits a faster acceleration, thus a reduction in take-off distance

- Easy to load and unload.

Disadvantage od tricycle undercarriage:

- Havier, because it takes greater load than tail wheel type

- Higher drag so must be retractable

- Static nose wheel reaction is about $6 - 16\%$ MTOW due to c.g. position and the nose unit must take 20 to 30% of the aircraft's weight in a steady braked condition and it is therefore relatively heavy

- High load on nose wheel makes it hard to rotate nose up on takeoff through an insufficient elevator power

- There is tendency for the aircraft to sit on its tail.

5.1 Undercarriage placement

The main gear is palced $7.2m$ from aircraft nose, to carry majority of the load on landing. The nose gear is paced $3.079m$ from the aircraft nose. To reduce weight and avoid additional frame and bulkhead in fuselage, the nose gear will be attached on front pressure bulkhead of fuselage, and main landing gear will be attached on fuselage frame.
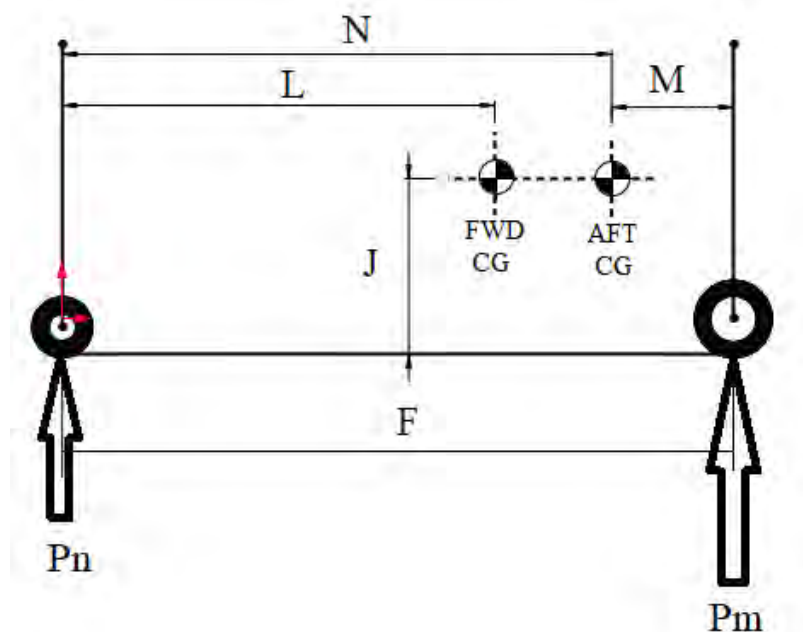
5.2 Tire size estimation

Figure 20: $F = 4.121m$; $L = 3.481m$; $M = 0.44m$; $N = 3.681m$; $J = 1.37m$

The main-wheel tire sizing are based on the most aft CG, nose-wheel tire sizing are based on the most forward CG position, the load on the wheels determine the tire size. To reduce landing gear weight and size, a single tire per strut was selected for both the nose and main gear.

Table 10: Tire loading

$W_{TO}(kg)$	4999
$P_M(kg)$	2791
$P_N(kg)$	970
$P_{N_{dynamic}}$	1616

Considering different tires from manufactures catalogue, the following tires were selected due to their load capacity and minimal dimensions.

Table 11: Tire types

	Tire	Outer diameter (in)	Width (in)	Ply rating	Speed index (mph)	Max. static load (kg)	Pressure (psi)
Main gear	Michelin type VII $(20x4.4in)$	20	4.4	14	255	2948	265
Nose gear	Michelin type VII $(16x4.4in)$	16	4.4	12	190	1598	207

5.3 Oleo strut sizing

Oleo pneumatic shock absorbers were selected due to their high shock absorption efficiency. The sturt dimensions are calculated according to the equation :

$$s_{sgp} = \frac{\frac{1.5\frac{W_L}{g}w_t}{\eta_s P_M N_g} - \eta_t s_t}{\eta_s} + \frac{1}{12} \tag{17}$$

where is

$$l_{sgp} \geq 2s_{sgp} \tag{18}$$

Table 12: Strut dimensions

	Nose strut	Main strut
N_g	5	5
w_t	$13 ft/s$	$13 ft/s$
η_t	0.47	0.47
η_s	0.8	0.8
S_s	$267 mm$	$398 mm$
l_s	$534 mm$	$796 mm$
d_s	$48 mm$	$73 mm$

and

$$d_s = 0.041 + 0.0025\sqrt{P_M}. \tag{19}$$

5.4 Undercarriage retraction and stow

After evaluation size of tires and shock absorbers we are able to find appropriates way of retraction of undercarriage and place in fuselage to stow wheels and struts (figure 21).
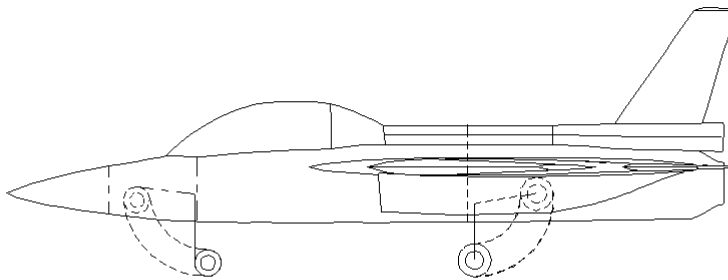
Figure 21: Undercarriage retraction

The nose strut will be retracted in fuselage bay between the radar and cabin bulkhead. The main struts will be retracted in side of fuselage, extended construction of intake.

5.5 Undercarriage criteria

Longitudinal criteria is defined:

$$A \geq 15°$$

$$A \geq B$$

like in the picture 22.

Figure 22: Longitudinal criteria

Lateral "tip-over" criteria can be seen in figure 23.

Figure 23: Lateral criteria

and defined is with angles below:

Criteria $\quad \psi \leq 55°$

In model $\quad \psi = 48°$

6 Weight and balance

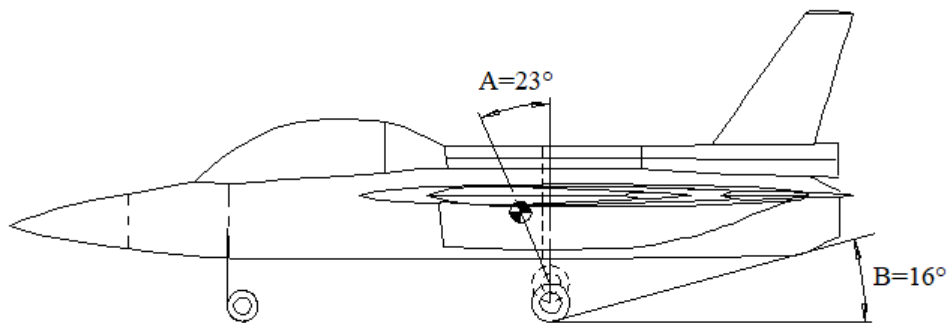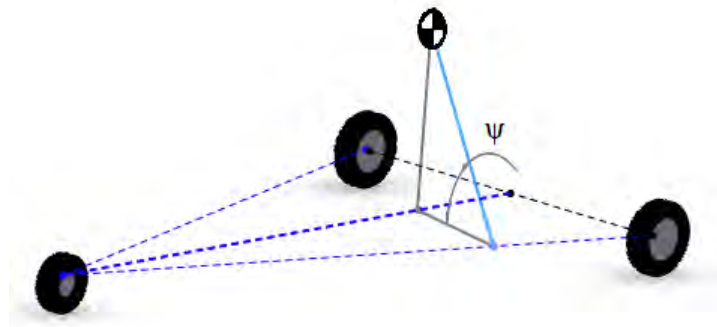The purpose of this chapter is to perform the weight and balance analysis of aircraft. A component weight buildup was performed to improve the accuracy of the total aircraft weight and determination of CG travel.

6.1 Component weight estimation

The weight of the components is determined by aircraft of a similar purpose, from statistically known component weight data.

Table 13: Component weight data

Component	Weight (kg)
Engine	620
Wing	487
Empennage	142
Fuselage	886
Undercarriage	266
Fixed equipment	827
Empty weight	**3228**
Crew	250
Trapped fuel and oil	25
Operating empty weight	**3503**
Payload	225
Fuel	1271
Take off weight	**4999**

6.2 *CG* travel

The following chart (figure 24) show weight and balance travel of the aircraft. Chart showes different loading conditions of aircraft, and for each condition, associated weight and center of gravity. For all loading conditions CG travel is less than 7% of M.A.C. The aircraft has the ability to fly from one military base to another with only one crew member.
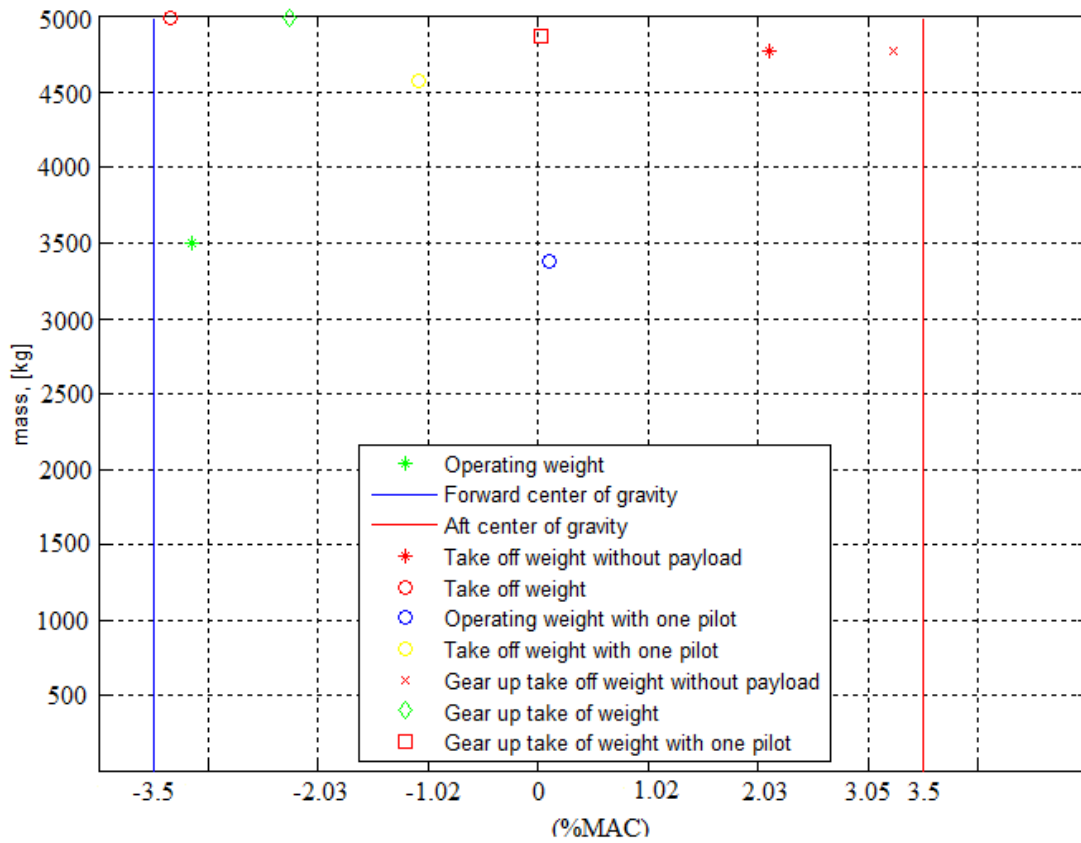
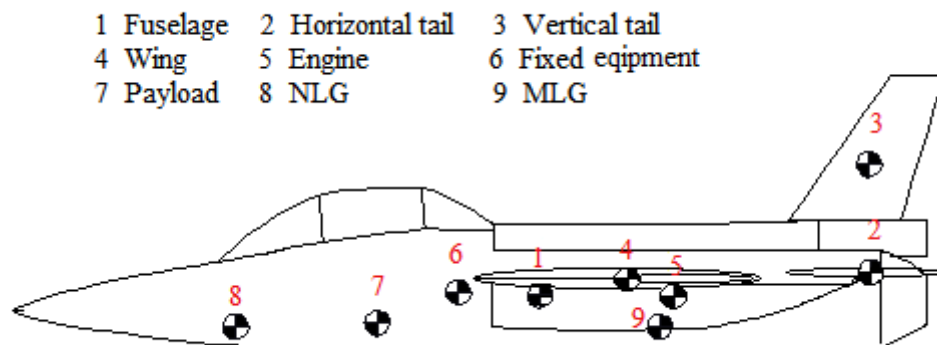Figure 24: Weight and balance travel

1	Fuselage	2	Horizontal tail	3	Vertical tail
4	Wing	5	Engine	6	Fixed eqipment
7	Payload	8	NLG	9	MLG

Figure 25: Side view of CG positions

7 Stability and control analysis

The process of aircraft stability analysis is divided into two parts: *Class 1* and *Class 2* (*Class 2* including dynamic stability analysis). Both of the methods used for the stability analysis will be shown in the further text.

7.1 *Class 1* method - static stability and control

7.1.1 Longitudinal static stability and control

Since this airplane has a 5th generation jet fighter training purpose, the decision was made that the airplane should be highly maneuverable, which implies that it should have low level of static stability and it is defined by the static margin:

$$SM = \overline{X}_{ac} - \overline{X}_{cg} \tag{20}$$

$\overline{X}_{ac}$ and $\overline{X}_{cg}$ are shown in picture 30.
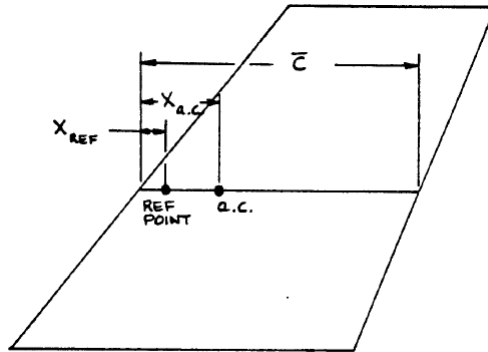
Figure 26: Aerodinamic symbols

The static margin value was calculated with respect to cruise conditions, at speed of Ma=0,7 and the height of 36000 feet (10058 m). Before the static margin could be calculated, the correlation between aircraft's aerodynamic center and horizontal stabilizer area had to be found. Aircraft's aerodynamic center is defined as: formula

$$\overline{X}_{ac_A} = \frac{\overline{X}_{ac_{wf}} + \frac{C_{L_{\alpha_h}}}{C_{L_{\alpha_{wf}}}}(1 - \frac{d\epsilon}{d\alpha})(\frac{S_h}{S})\overline{X}_{ac_h}}{1 + \frac{C_{L_{\alpha_h}}}{C_{L_{\alpha_{wf}}}}(1 - \frac{d\epsilon}{d\alpha})(\frac{S_h}{S})}. \tag{21}$$

While analysing weights and balances, all possible scenarios of weight distribution had to be taken into consideration. Two critical cases were defined including most aft position (full tank and 1 crew member) and most forward position (2 pilots and an empty fuel tank) which gave two different C.O.G. positions. Using the *MATLAB* software, further calculations regarding the static margin with respect to horizontal stabilizer are were made. The results are shown in figure 27.
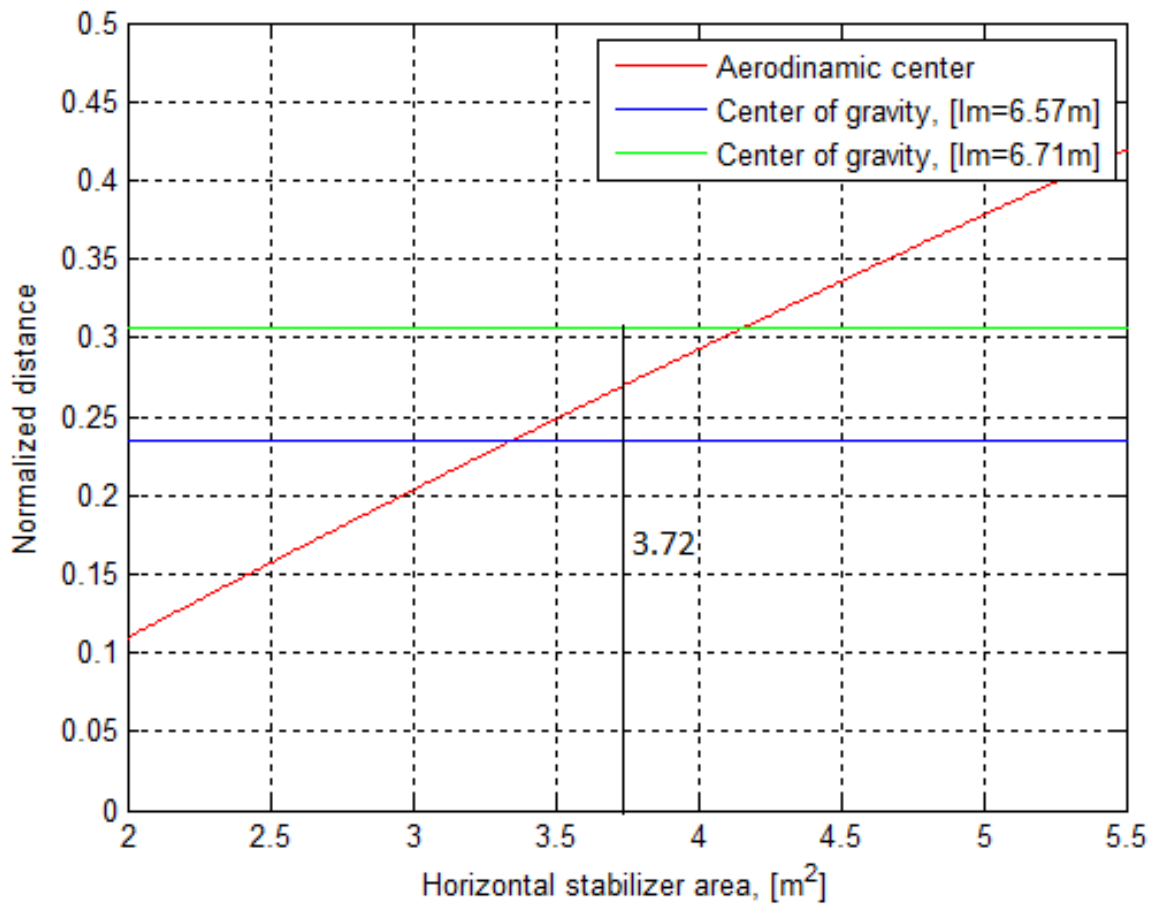
Figure 27: Static margin

Previous calculations resulted with the static margin value of 3.3% M.A.C. for the most forward position of C.O.G. and - 3.9% M.A.C. for the most aft position using the horizontal stabilizer area value of $3.72m^2$. Since this aircraft has a jet fighter training purpose, it's static margin should be no less than -5% M.A.C. according to Roskam [2]. It is possible to conclude that the aircraft will be statically stable in the first scenario which won't be the case in the second scenario. The problem of static instability in the second scenario will be solved using the

closed loop flight control system. The feedback gain value of $1.77°/°$ needed to compensate the longitudinal instability problem for the most aft position of the C.O.G. was found satisfactory since it doesn't exceed maximum feedback gain value of $5°/°$ [2]

$$k_\alpha = \frac{(\Delta SM)C_{L_\alpha}}{C_{m_{\delta_e}}}. \tag{22}$$

Interconnection between the horizontal stabilizer area and longitudinal feedback gain value can be found in figures 28.
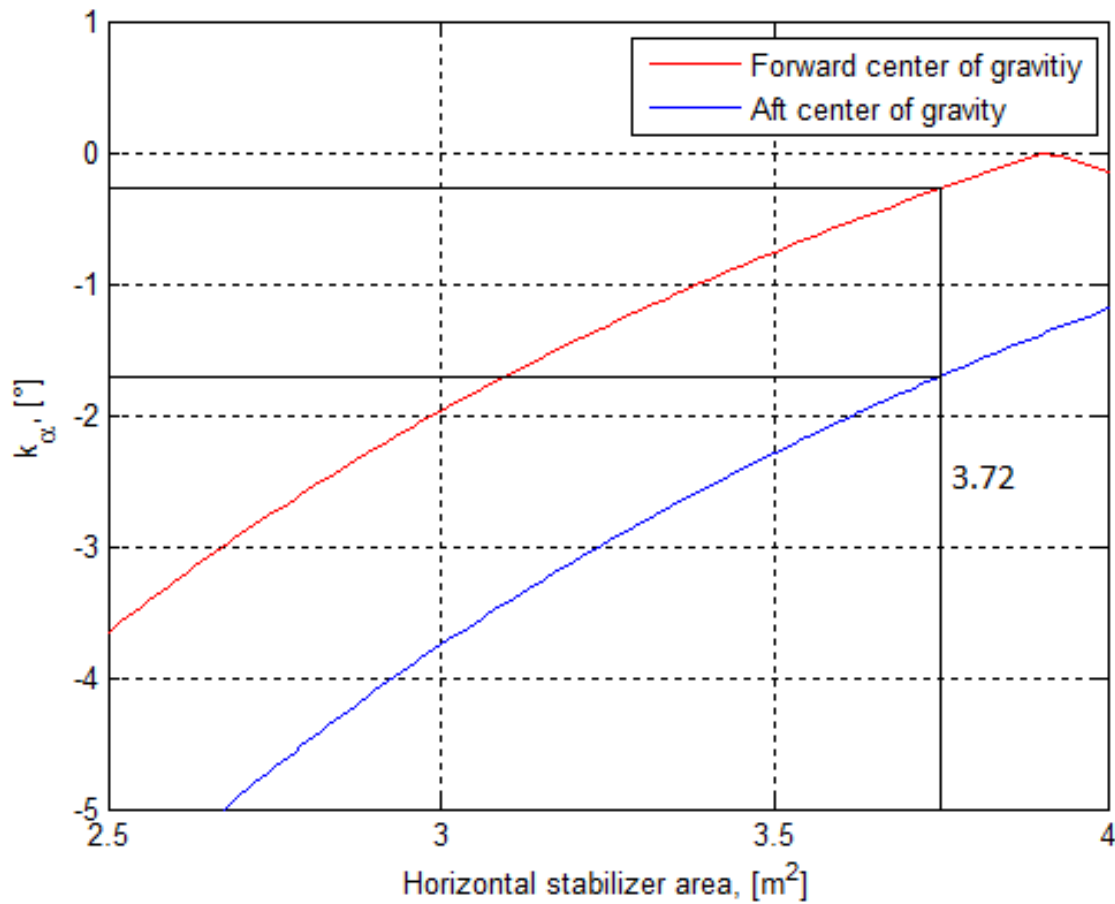

Figure 28: Feedback gain

Using the horizontal stabilizer area value $Sh = 3.72m^2$, following longitudinal feedback gains for the most forward and most aft positions were found:

$$(k_\alpha)_{forward} = -0.33°, \tag{23}$$

$$(k_\alpha)_{aft} = -1.77°. \tag{24}$$

43

7.1.2 Lateral static stability and control

After defining the yaw moment derivative due to sideslip angle:

$$C_{n_\beta} = C_{n_{\beta_w}} + C_{n_{\beta_f}} + C_{n_{\beta_v}}, \tag{25}$$

it is possible to calculate the rudder feedback gain value, defined as:

$$k_\beta = \frac{(\Delta C_{n_\beta})}{C_{n_{\delta_r}}} \tag{26}$$

Interconnection between the vertical stabilizer area and longitudinal feedback area is shown in the figure 29.
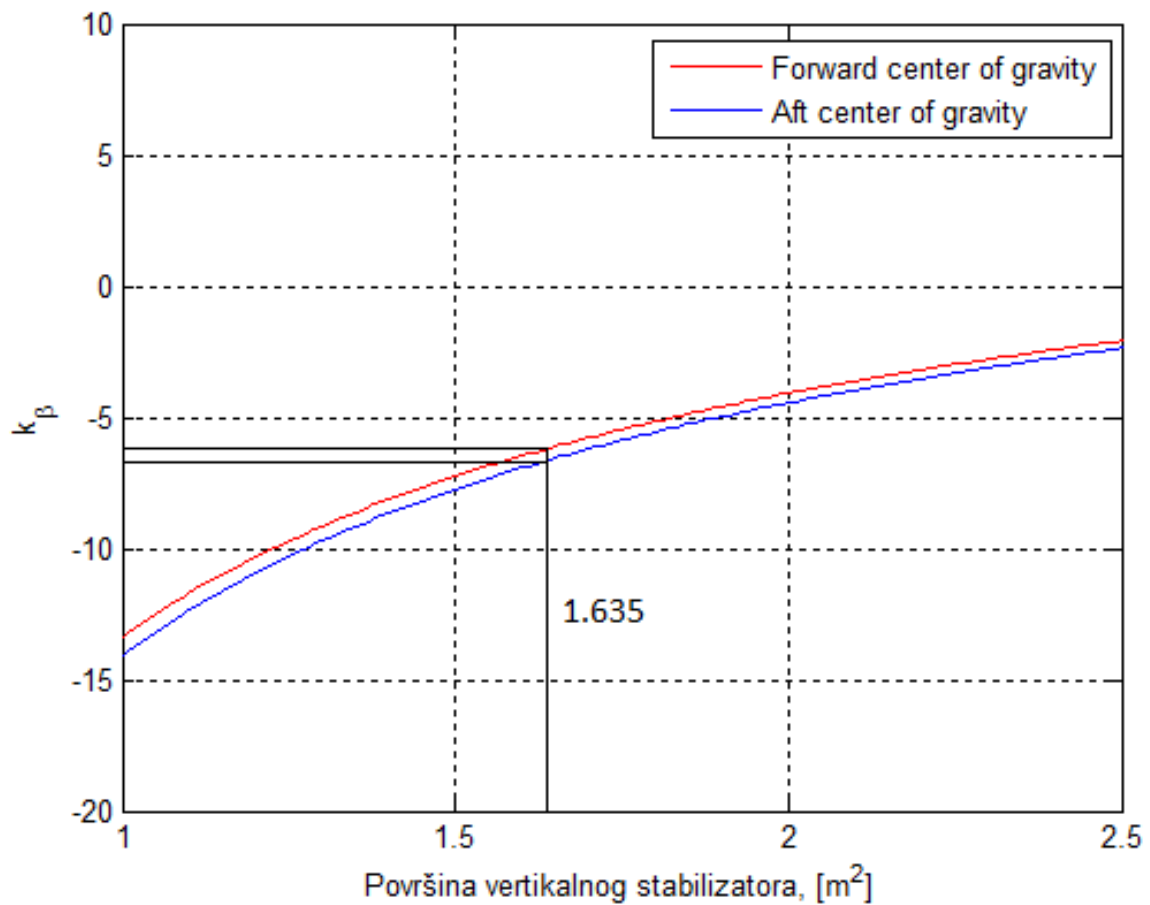

Figure 29: Rudder feedback gain

It was found that the vertical stabilizer didn't give enough contribution to directional stability (the rudder feedback gain value exceeded $5°/degree$), it's surface had to be increased enough to result with the satisfactory value of rudder feedback gain. Due to the difference more than

10% from the original value of the vertical stabilizer, center of gravity had to be recalculated and it was found out that it moved backwards for a very small value, so the calculations could be continued. Furthermore, the rudder feedback gain value was found to be satisfactory, but still pretty high, which wasn't considered to be a problem since it should result in high lateral maneuverability. Both, longitudinal and directional static stability calculations were made using the *MATLAB 2015* software.

7.2 *Class 2* method - dynamic stability and control

Dynamic stability and control calculations were made using the *CEASIOM* software, but since *CEASIOM* uses *.xml* and *.txt* files only, a new parametric *.xml* model had to be made for that purpose. A few minor corrections had to be made while designing the geometry in *CEASIOM* due to the fact that the model made with *CEASIOM* represents only an aerodynamic approximation of the real CAD model which serves for the dynamic stability calculation purposes only.
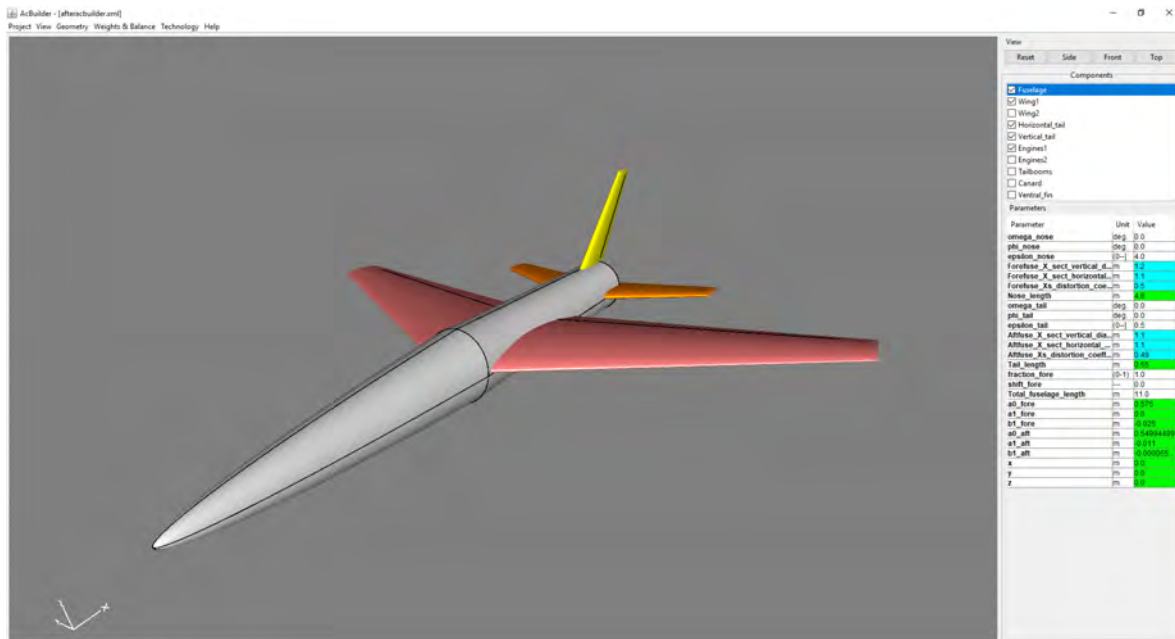

Figure 30: Airplane geometric model

The following results are computed for the cruise regime which is accomplished at the height of 36,000 ft (10058 m) at the speed of Ma=0.70. Firstly, the trim AOA had to be found which was computed by solving the system equilibrium equations, which are actually the sum of moments

and forces acting upon the aircraft during the cruise regime. The trimmed angle of attack value was found to be $[\alpha_{trim}] = 0.86°$, with the corresponding value of elevator deflection which was found to be $[\delta_e] = 9°$.

Now, when the trimmed AoA and elevator deflection are found, it is posible to extract the stability derivatives using the *CEASIOM* software. Stability derivatives can be easely read in figure below:
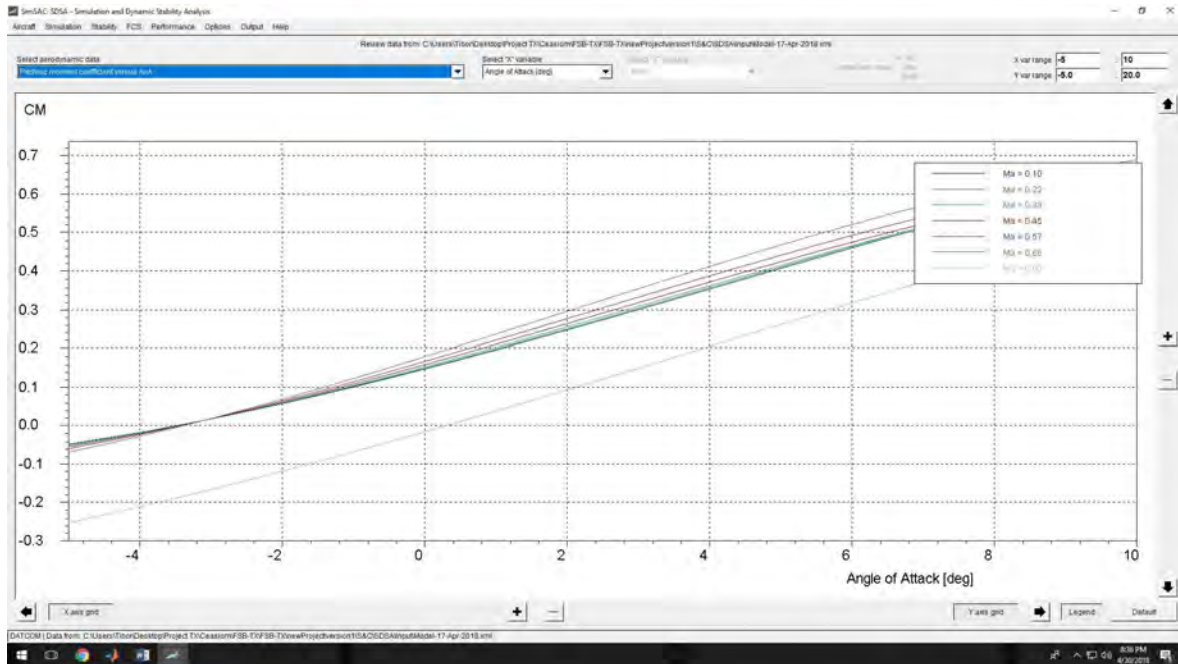

Figure 31: *Ceasiom* derivative

The following table contains dynamic stability gradients for the cruise regime mentioned earlier.

Table 14: Stability derivative

Derivative	Value in cruise regime
C_m	0.225
C_L	0.23
C_D	0.0113
C_{y_β}	-0.595
C_{l_β}	-0.078
C_{n_β}	0.133
C_{z_q}	2.73
C_{m_q}	-11.7
C_{l_p}	-0.35
C_{n_p}	-0.017
C_{n_r}	-0.136
$C_{m_{\delta_e}}$	-0.67
$C_{l_{\delta_l}}$	-0.104
$C_{Y_{\delta_r}}$	0.442
$C_{l_{\delta_r}}$	0.0369
$C_{n_{\delta_r}}$	-0.181

Since the airplane itself isn't statically stable in this regime (assuming full fuel tanks and 2 pilots), a closed loop feedback system had to be introduced to the model to assure "de facto" stability (figure 32). Using the calculations which were made in the static stability analysis, the values of pitch and yaw feedback gains are known and will be implemented to the *CEASIOM* aerodynamic model. The implementation is done directly using the *CEASIOM* user interface which allowed further analysis of dynamic stability characteristics of the aircraft. The influence of the pilot on the dynamic behaviour wasn't included in the simulation.
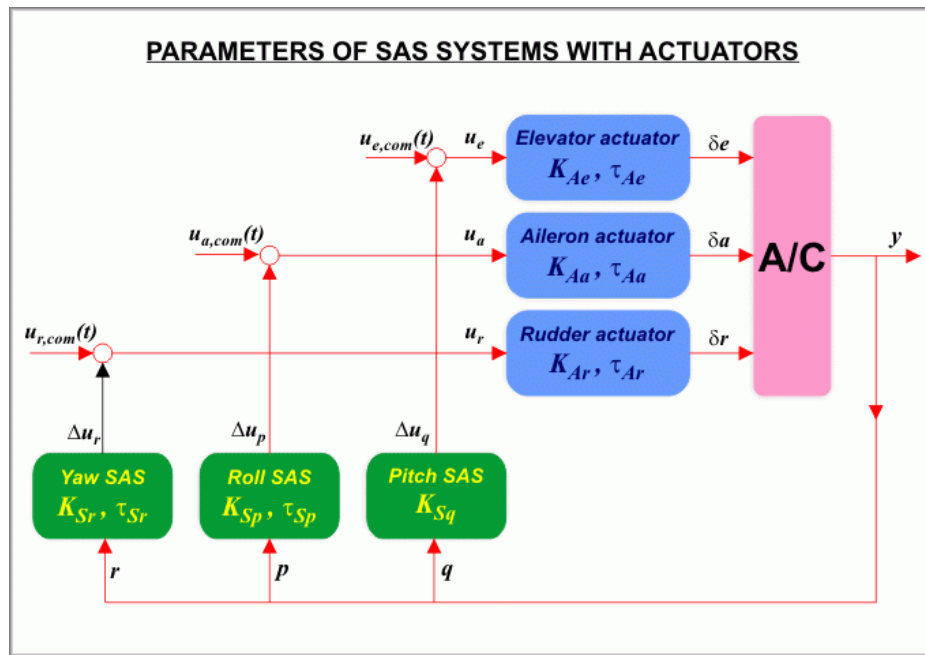
Figure 32: Closed loop feedback system

Once the feedback gain values for pitch and yaw were introduced to the model, the stability criteria calculations according to MIL-F-8785-C, Class IV (high maneuverability airplanes) standard could be completed. Furthermore, the results for the phugoid mode, roll, spiral, and dutch roll mode will be shown, comparing the values with and without the closed loop flight control system (figure 32). Various feedback gain values for the yaw and pitch to determine which value would give the best response results. After the analysis had been done, three feedback gain values were chosen. The yaw feedback gain value was found to give the best results at 4.9, pitch feedback gain value is 1.45 and roll feedback gain value was only 1.

The picture 33 represents the graph of damping ratio with respect to TAS, with minimum damping ratio limit according to MIL standard MIL-F-8785-C for high maneuverability airplanes. The aircraft shows satisfactory results for all TAS values taken into consideration.

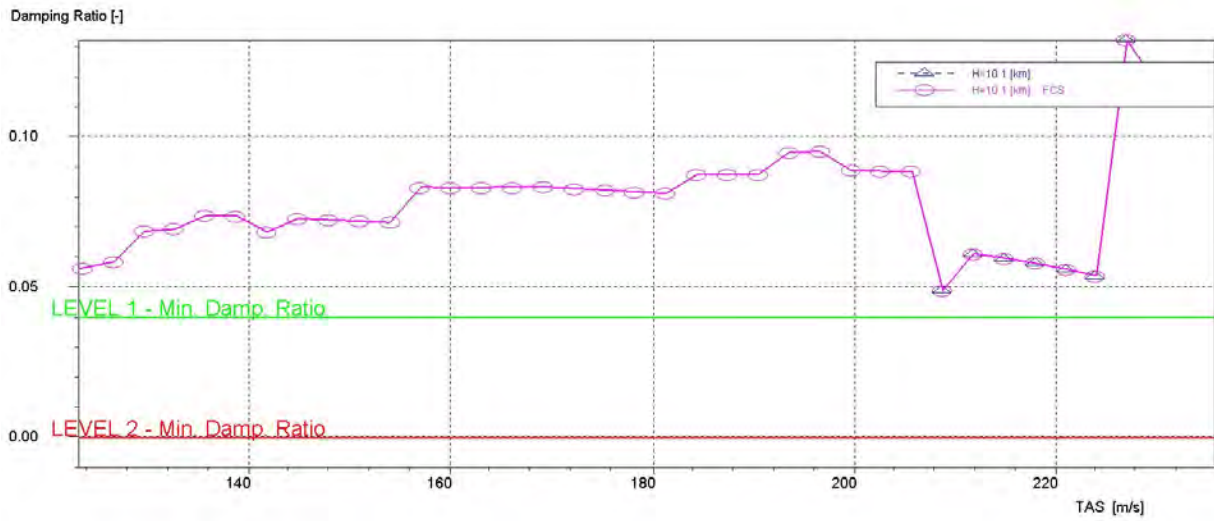Figure 33: Phugoid mode damping ratio with respect to TAS (MIL standard)

The figure 34 represents the damping ratio with respect to undamped natural frequency for all the TAS values mentioned before. The results aren't varying much and one could conclude that, according to MIL-F-8785-C standard, this airplane falls into Level 2 category for the dutch-roll mode, which is found to be satisfactory.

Figure 34: Dutch roll
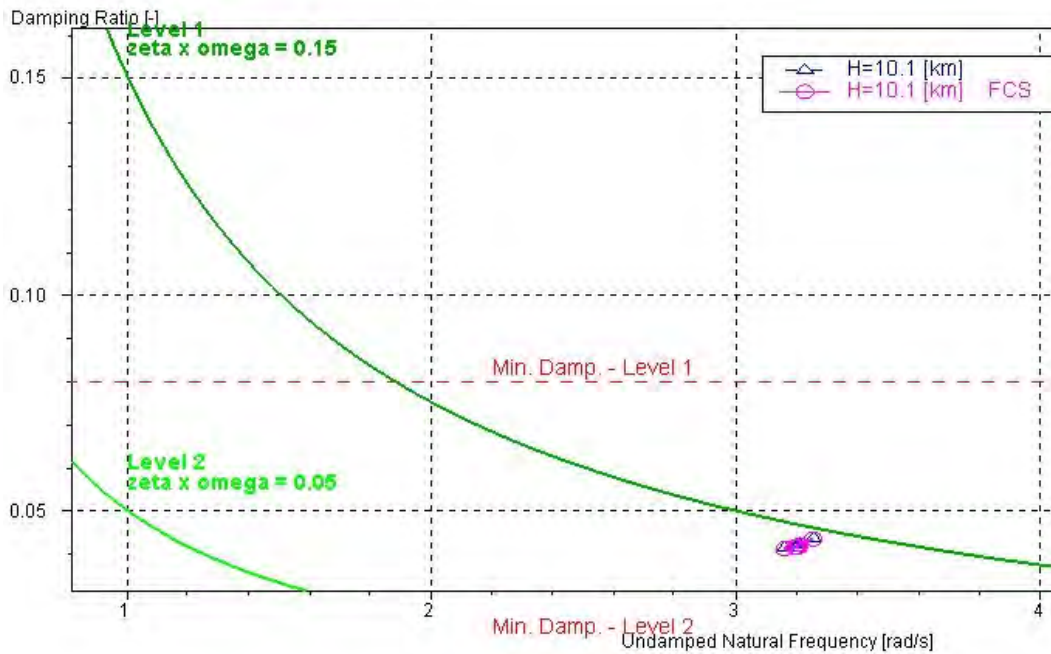
According to Cooper-Harper (figure 35) pilot assessment rating, there is much space for the improvements regarding the dynamic stability of the rolling mode. Since it is satisfactory according to MIL-F-8785-C and it would require thorough analysis which would be time consuming, further improvements will be left for the future analysis.
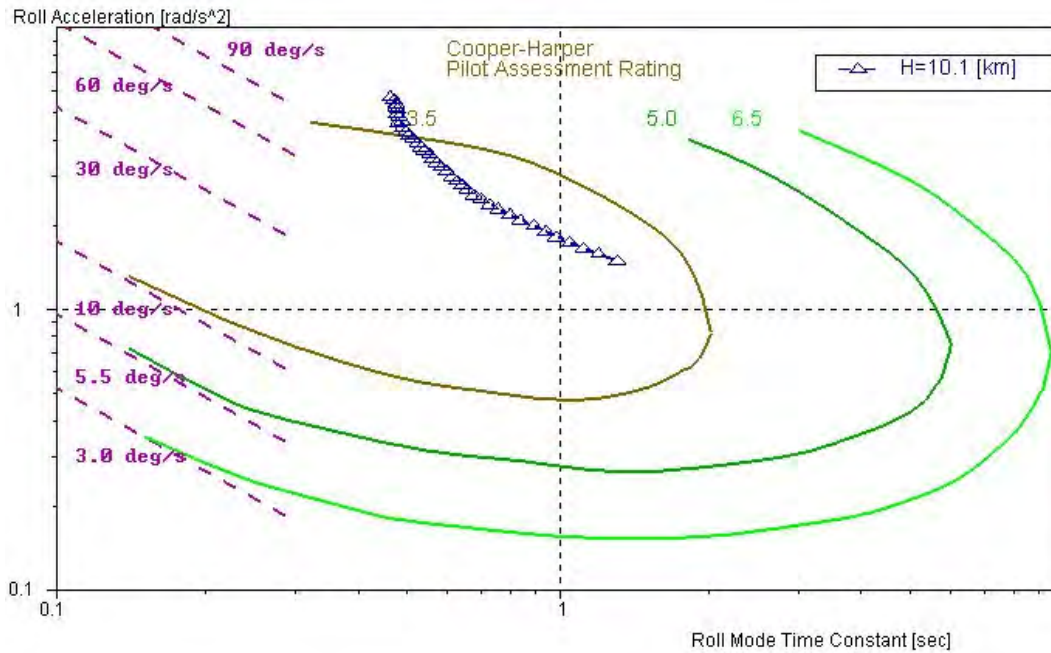

Figure 35: Cooper-Harper pilot assessment rating

8 Aircraft Performance

Performance analysis consists of a number of cases required for the current proposal. First case includes take-off and landing distance at max gross weight including standard day and icy runway balanced field length at sea level. Since this is a single-engine aircraft, runway length requirements would be approximated by adding take-off and landing distance together. Second case will show climb and ceiling performance. Third case demonstrates aircraft maneuvering at 4572 m (15000 ft) within several examples of load factor. Fourth case demonstrates cruise, range and endurance requirements. Besides all of this cases, this chapter includes maximum Mach Number at 10972.8 m (36000 ft), 1-g and 5-g Maximum Thrust Specific Excess Power Envelope, Energy Maneuverability Diagram at 15,000 ft MSL, L/D vs Mach at 10972.8 m (36000 ft) and V-n diagram showing response to 9.144 m/s (30 ft/s) equivalent sharp-edged vertical gust.

8.1 Take-off and Landing distance requirements

Take-off and landing requirements are one of the most critical variables that determined the aircraft layout. This requirements depends on aircraft aerodynamics, powerful engine and weight. All this requirements are considered on icy runway with maximum gross weight of the aircraft. To perform take-off and landing analysis, key aircraft speeds must be determined. Minimum speed is 1.1/1.2 higher than aircraft stall speed in Take-off/Landing configuration. All values according take-off and landing requirements are given in Table 15.

Table 15: Take-off and landing requirements

	TAKE-OFF	LANDING
V_{stall}, m/s	58.953	55.149
V_{LOF1}, m/s	64.849	-
V_{LOF2} to pass 50ft obstacle, m/s	76.639	-
V_{TD}, m/s	-	62.782
V_A, m/s	-	66.178
s_{TOG}, m	292.609	-
s_{TO} with 50ft obstacle, m	408.686	-
s_{AIR} from 50ft obstacle, m	-	375.515
s_{LG}, m	-	502.010
$s_L=s_{AIR}+s_{LG}$, m	-	877.526

As can be seen from the Table 15, adding take-off and landing distance together is equal to $s_{TO}+s_L$=1286.212 m or 4219.804 ft, which meets RFP conditions.

8.2   Climb

Climb performance is shown on Figure 36 and 37. It demonstrates climb performance with maximum gross weight. Rate of Climb is shown after take-off, in clear configuration with Mach number 0.5 and 0.7 as well as time to climb. Maximum rate of climb is reachable at altitude of 0 m with higher possible Mach number. Time to 10973 m is 4.5 min at an initial climb rate of 180 m/s.
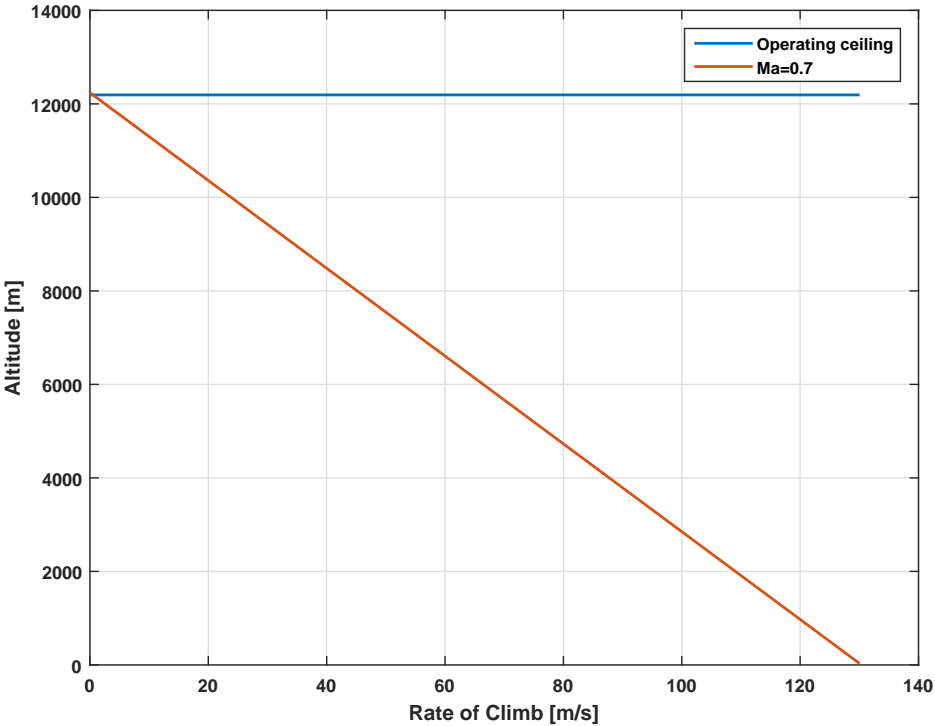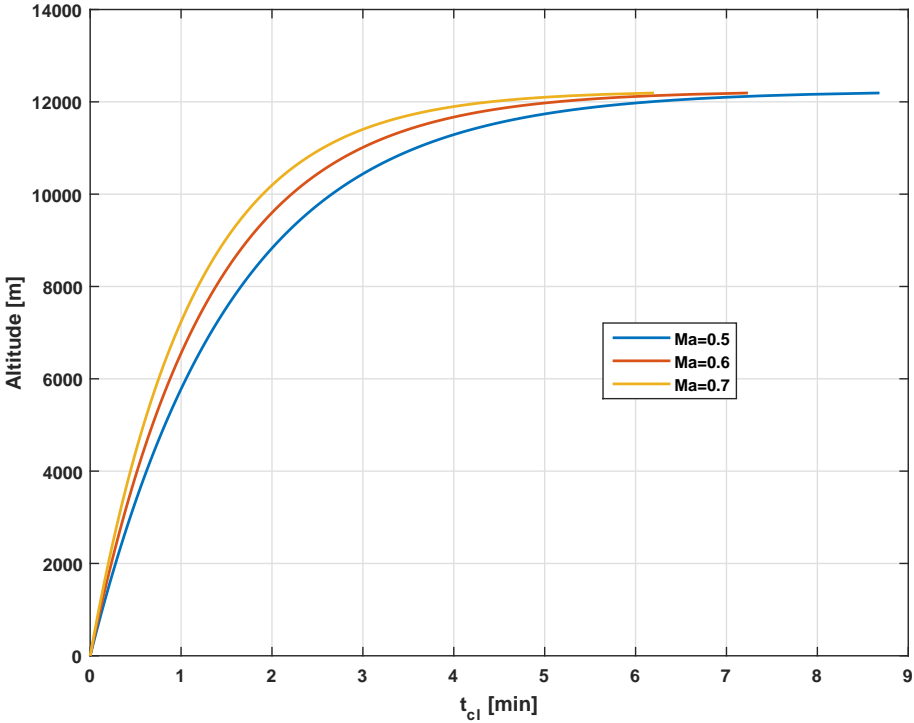
Figure 36: Rate of Climb with Altitude

Figure 37: Time to Climb with Altitude

8.3 Range and endurance

Payload range curves were obtained using Breguet range formula with constant cruise Mach number and three different altitudes as shown on Figure 38. In this case, range is simplified, and it is enough to show that aircraft will reach at least minimum distance requirement. Endurance curves were obtained with three different altitudes too. As it is shown on Figure 39, maximum endurance is reachable at Mach=0.55.

Figure 38: Range

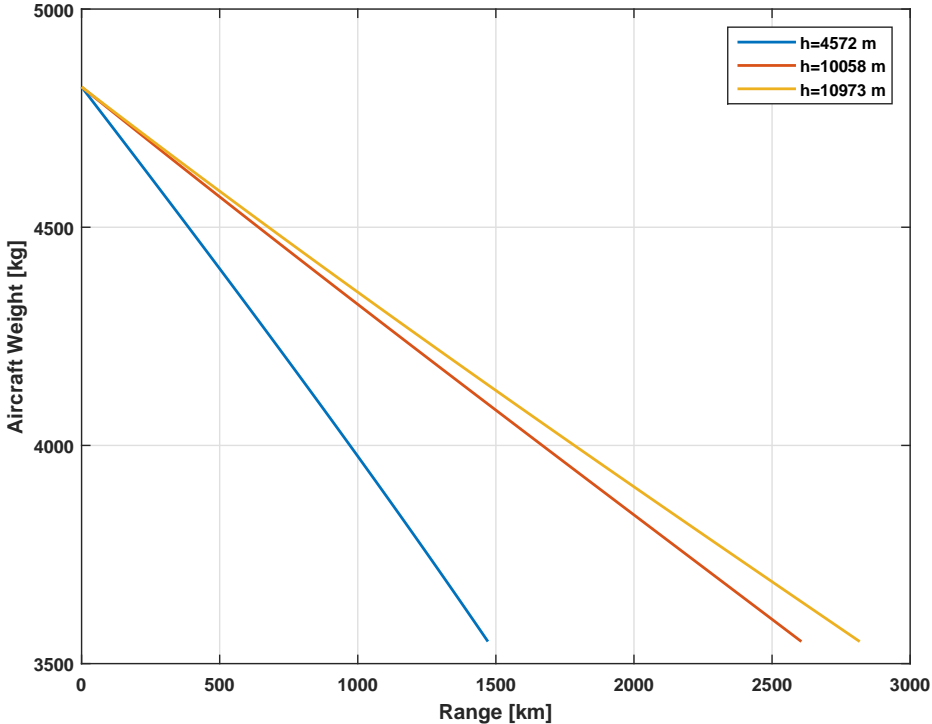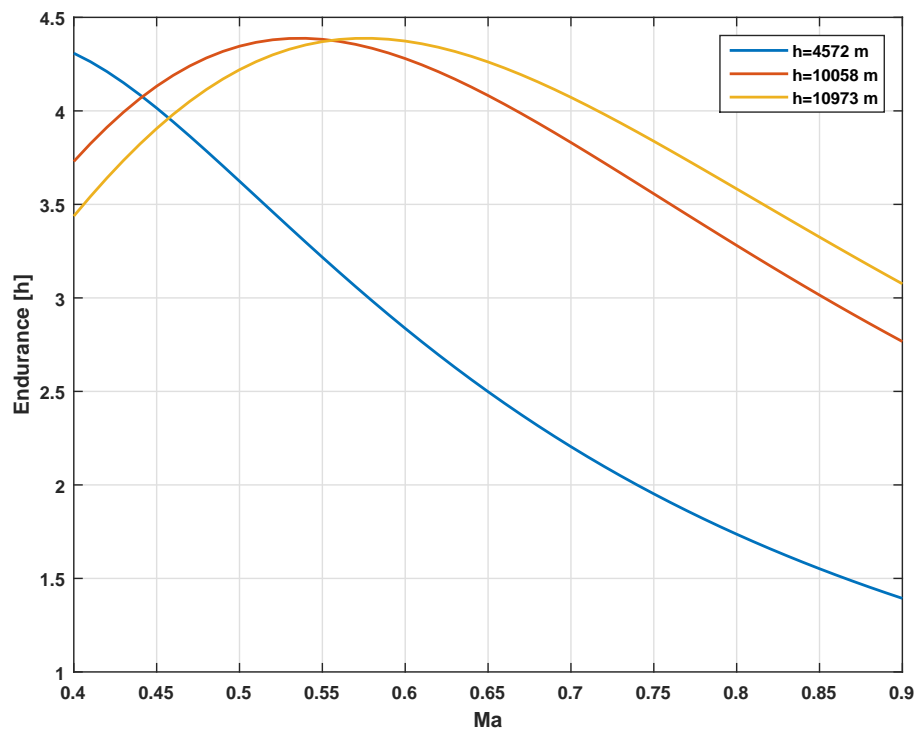Figure 39: Endurance

8.4 Maximum Mach Number at 10058 m (36000 ft) and wave drag

Wave drag was analysed with OpenVSP software (Figure 40). Drag below critical Mach number can be computed from aerodynamic equations. Wave drag can be analysed with OpenVSP software for Mach greater than 1.0. Numbers around Mach 1 are difficult to compute and wave drag is more accurate for higher Mach values.
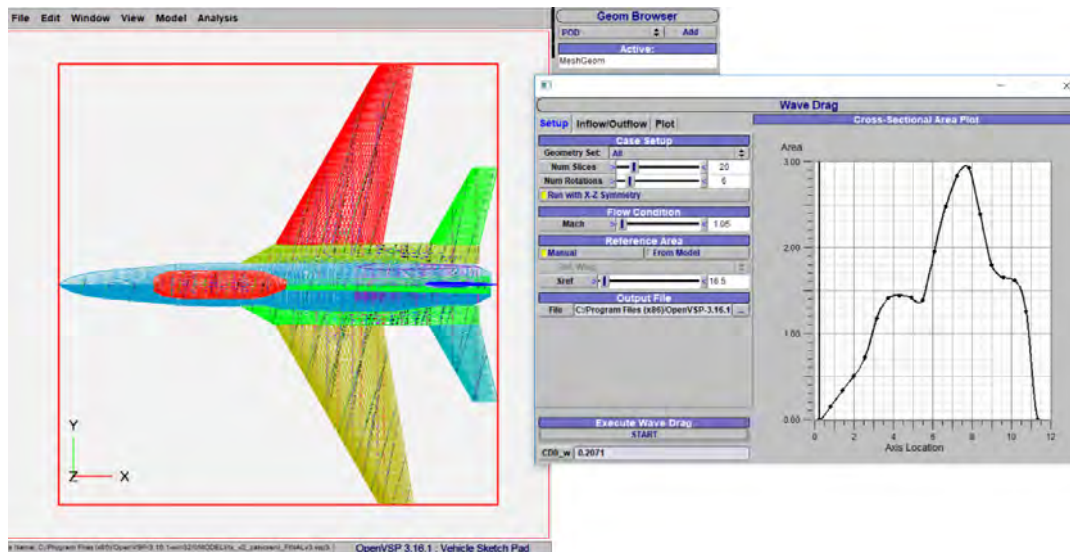
Figure 40: Wave Drag shown in OpenVSP

Because of that, in transonic flight, total drag needs to be approximated by following procedure:

1. first point is where the wave drag starts to grow from 0, on diagram that is at Mach 0.85

2. most accurate supersonic point is the drag value at Mach 1.2.

3. with rest of the points as orientation values, continuous curve is drawn.

That analysis provides enough accurate results for this stage of design. 41 shows the result of described procedure. Except total drag, on 41 is the maximum thrust expressed as corresponding drag coefficient value which can be achieved with this aircraft and chosen engine. Intersection of orange and black curve is around Mach 0.95 which represents the maximum Mach number at 36,000 feet. That is also the Dash speed of the aircraft in level flight.
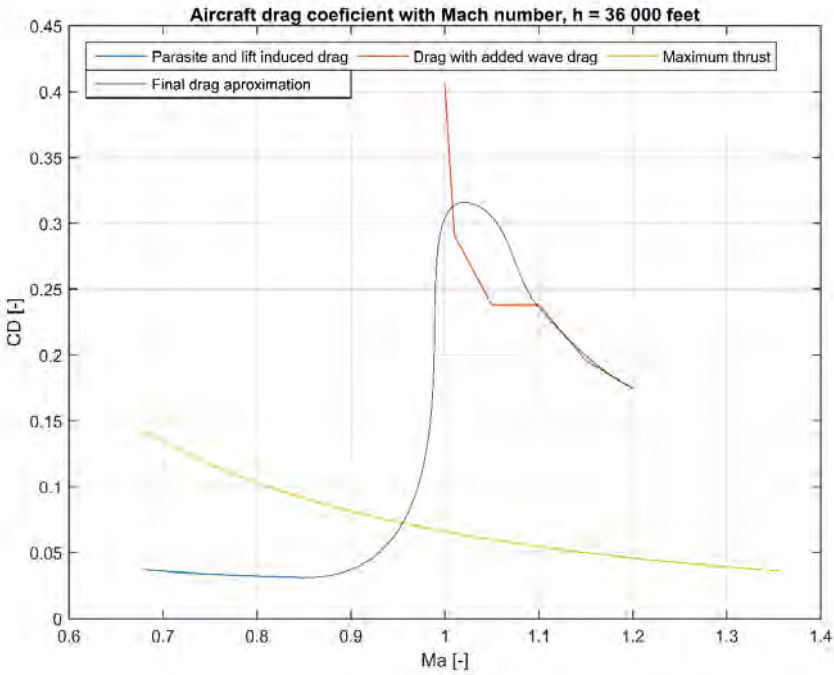
Figure 41: Drag coefficient with Mach number

8.5   1-g Maximum Thrust Specific Excess Power Envelope

Given diagram on Figure 42 shows that aircraft has enough power to fly at the large span of speeds and heights. Maximum (dash) speed is at Ma=0.95, and maximum altitude is around 10058 m (40 000 ft). Red line represents stall speed. Values on the circular lines represent constant available Rate of Climb. Diagram represents operative envelope with operative ceiling of 12192 m (40000 ft).
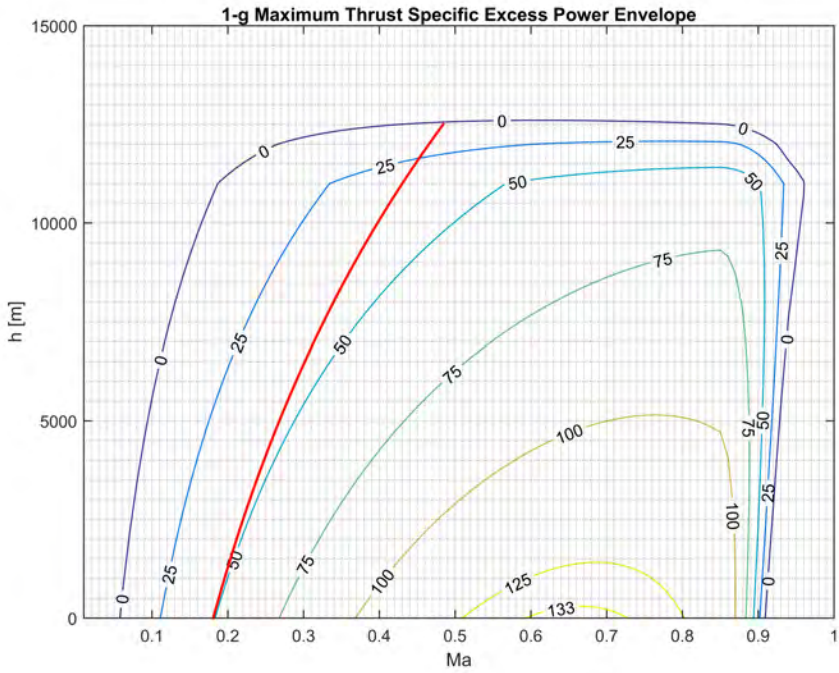
Figure 42: 1-g Maximum Excess Power Envelope

8.6 5-g Maximum Thrust Specific Excess Power Envelope

Diagram on Figure 43 shows that aircraft will have enough power to make required 5-g manoeuvres till 4572 m (15 000 ft) of altitude. Higher g numbers are possible thanks to the structure, but they need to be performed with aircraft in descend.
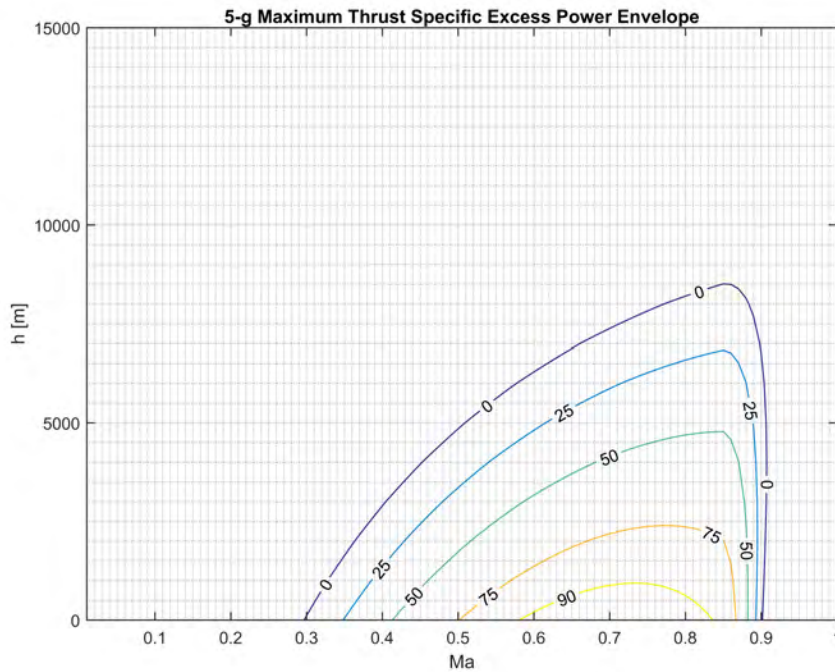
Figure 43: 5-g Maximum Excess Power Envelope

8.7 Energy Maneuverability Diagram at 4572 m MSL

To demonstrate aircraft maneuverability, it is important to show characteristics such as turn radius and turn rate. Since this is trainer aircraft, which will show the characteristics of some combat aircraft, it is necessary to show that it will be able to achieve small turning radius as well as high turning speeds. This diagram shows relation between turn rate in degrees per second and Mach Number. Full lines are for constant g-load, while dashed lines are for constant turn radii in meters. Bold dashed lines represent the limits – from left side limit is stall speed, from right side maximum speed (Mach Number) and from above is maximum sustained load on a structure.
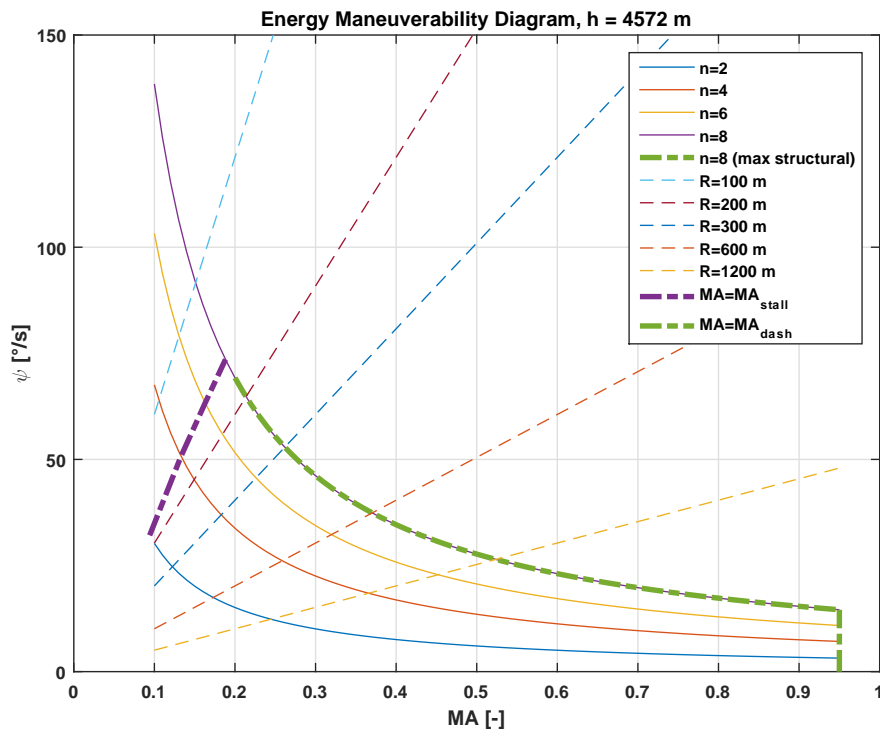
Figure 44: Energy Maneuverability Diagram

8.8 L/D vs Mach at 10058 m (36000 ft)

Best L/D ratio for given aircraft in level flight at 10058 m is $(L/D)_{max} = 10.888$ at Mach=0.5386. 45 shows the diagram for rest of the Mach numbers at 10058 m. Diagram stops at 0.85 where wave drag occurs and L/D starts to decrease rapidly.
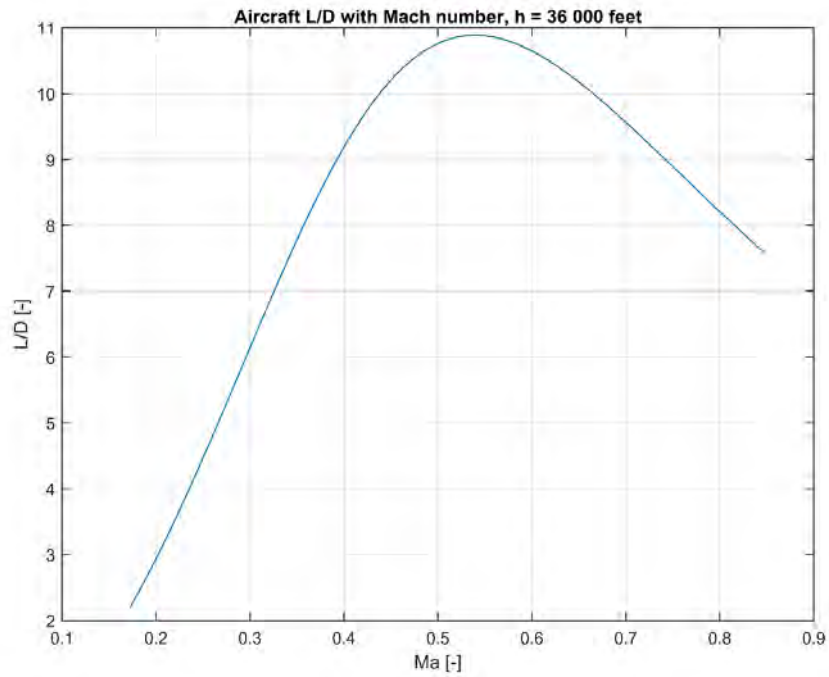
Figure 45: L/D with Mach number

Table 16: Aircraft Specifications

Dash speed at 10973 m, -	0.95M
Cruise speed at 10973 m, -	0.7M
Maximum Range at 10058 m, km	2800
Maximum Endurance at 10973 m, h	4.4
Maximum Rate of Climb (Initial), m/s	130
Service ceiling, m	12192
Take-off runway length, m	408.69
Landing runway length, m	877.53
Sustained g at 4572 m MSL, -	8
Payload, kg	226.8

9 Cost estimation

In this chapter, we will estimate the total life cycle cost of the aircraft, further dividing it into non-recurring cost such as research, development and testing as well as recurring cost such as acquisition, operation and disposal costs[1]. Per unit production cost, as well as per unit flyaway cost will be estimated. All presented estimates are expressed in 2018 USD.

9.1 Research, Development, Test and Evaluation cost

The research, development, test and evaluation (RDTE) cost is a non-recurring cost that accounts for most of the cost of an aircraft program The following assumptions are made:

- 8 aircraft produced for RTDE of which one is an iron bird,

- Knowledge of CAD tools,

- The aircraft will be fitted with existing technologies and systems,

- No aircraft stealth requirements,

- Available manufacturing and research facilities,

- RTDE profit of 10 percent,

- Interest rate of 10 percent.

The total non-recurring cost of research, development, test and evaluation is approximately **464,000,000.00 USD**. Figure 46 shows the contribution of certain items to the total RTDE price.
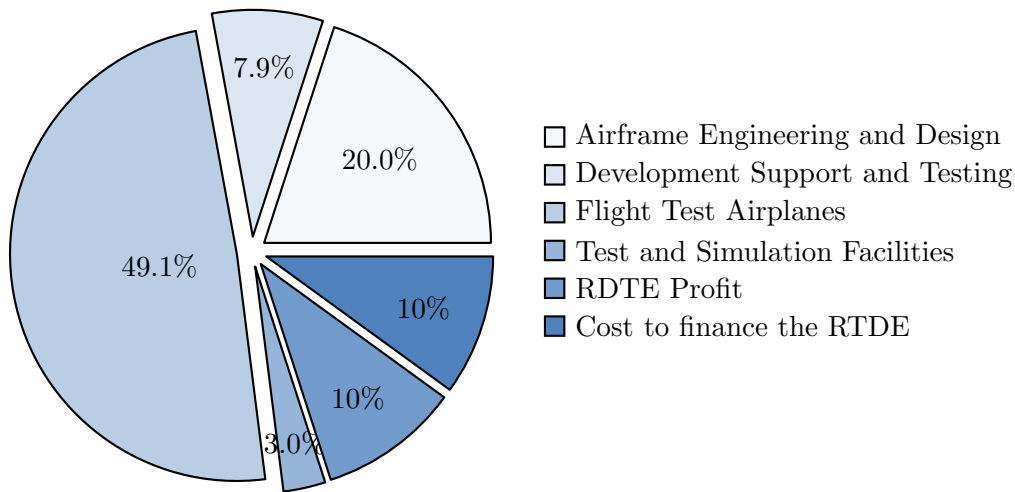
Figure 46: Contribution of certain parts to the total RDTE price

9.2 Manufacturing and Acquisition Cost

Figure 47 shows the contribution of certain items to the total Manufacturing and Acquisition price for a production run of 500 aircraft. Figure 48 shows the Manufacturing and Acquisition cost depending on the number of aircraft manufactured.
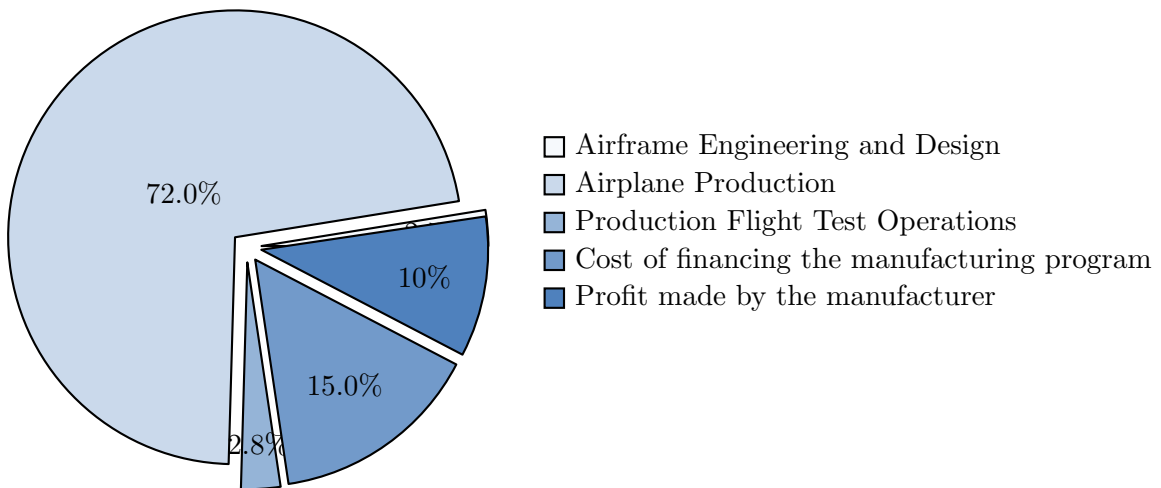
Figure 47: Contribution of certain parts to the total Manufacturing and Acquisition price
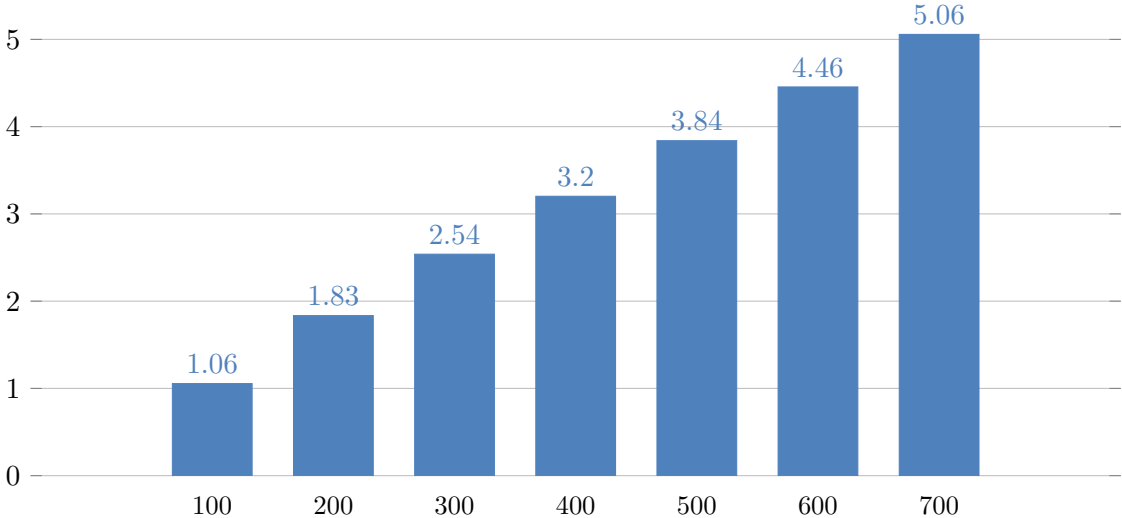
Figure 48: Price of Manufacturing and Acquisition depending on the number of produced aircraft; price in billion of USD

9.2.1 Flyaway cost

Flyaway cost is the cost per aircraft including manufacturing and tooling but excluding RTDE. Figure 49 shows the flyaway cost per unit depending on the number of aircraft produced.
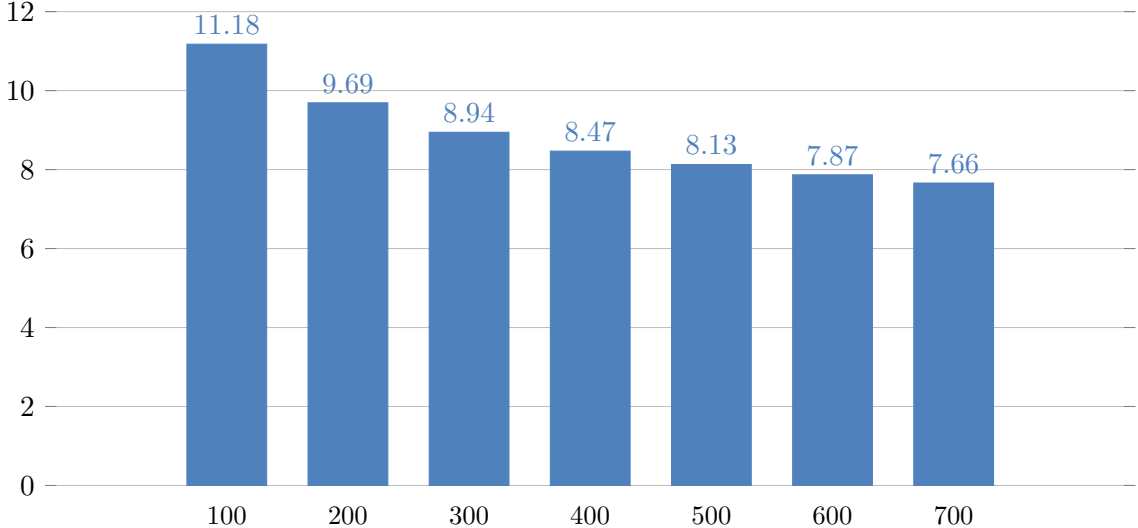
Figure 49: Flyaway cost per unit depending on the number of produced aircraft; price in million of USD

9.2.2 Per Unit Cost

Per unit cost is the total cost of the project divided by the number of aircraft produced. Figure 50 shows the per unit cost depending on the number of aircraft produced.
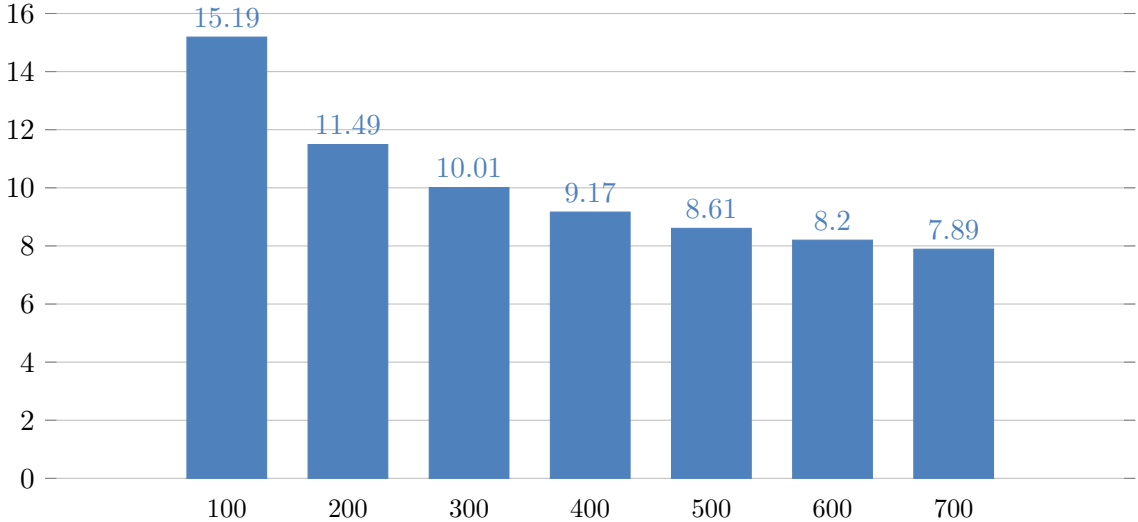
Figure 50: Per unit cost depending on the number of produced aircraft; price in million of USD

9.3 Operational cost

Some assumptions have been made when estimating the operating cost of the aircraft:

- A fuel price of 2.113 USD/gal, as of April 2018.,

- 30 year active service life with 1,000 flight hours per year per airplane,

- A loss rate of 1.5 aircraft per 10^5 flight hours

- 6 maintenance hours per flight hour due to the easily serviceable construction

Figure 51 shows the contribution of certain items to the Operating cost. Figure 52 shows the Operating cost depending on the number of produced aircraft. The operating cost per hour is approximately 2,650 USD.
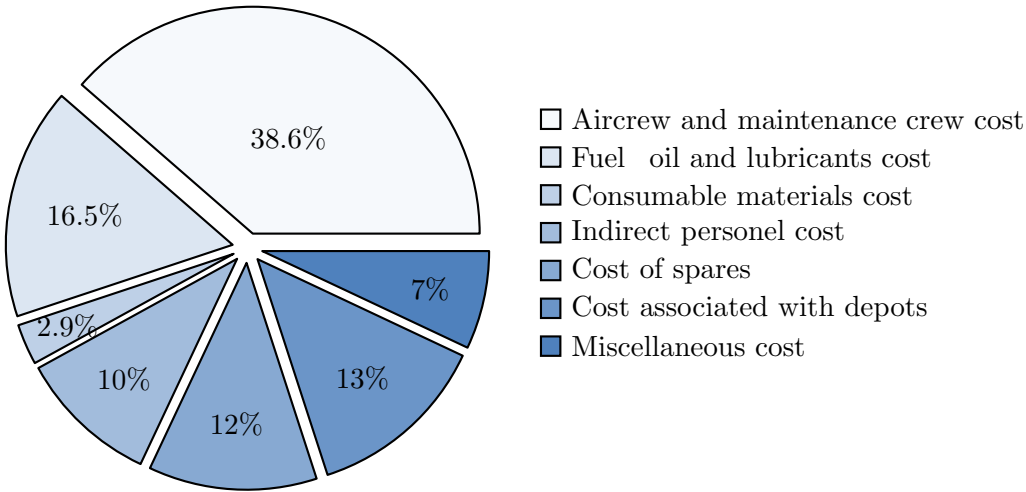
Figure 51: Contribution of items to the Operating cost
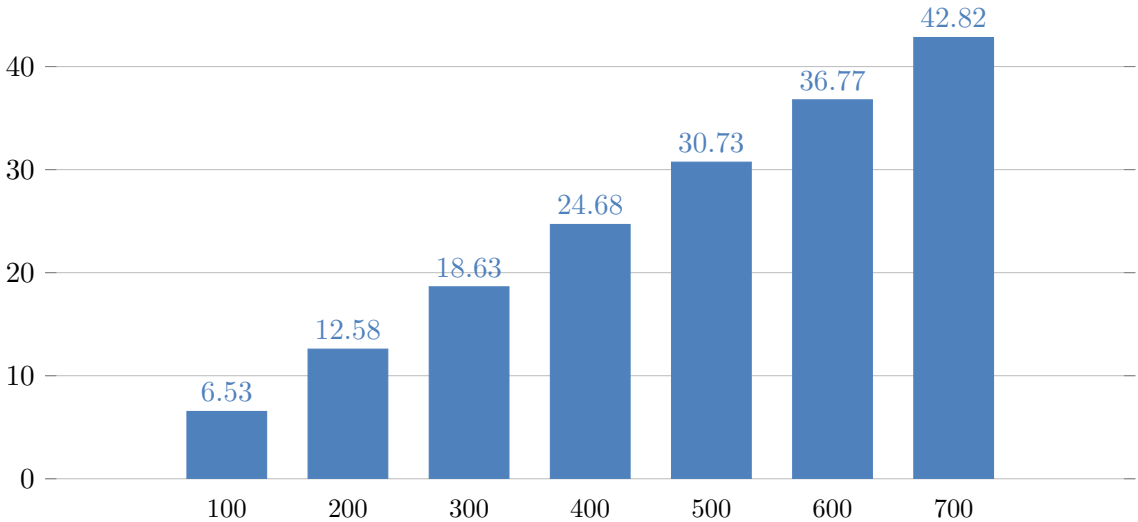
Figure 52: Operating cost depending on the number of produced aircraft; price in billion of USD

9.4 Life cycle cost

Life cycle cost of an airplane program (LCC) is the total cost of developing, purchasing, operating and disposing of a fleet of aircraft. Figure 53 shows the Life cycle cost depending on the number of produced aircraft. Figure 54 shows the items contributing to the Life cycle cost on an example of a production of 500 aircraft. The disposal cost is assumed to be 1% of the life cycle cost.
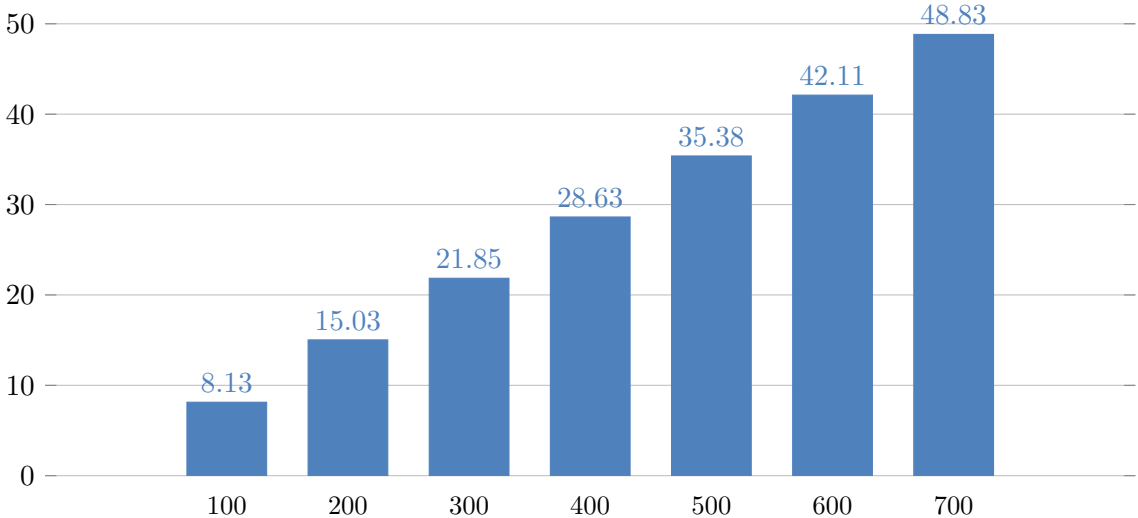
Figure 53: Life cycle cost depending on the number of produced aircraft; price in billion of USD
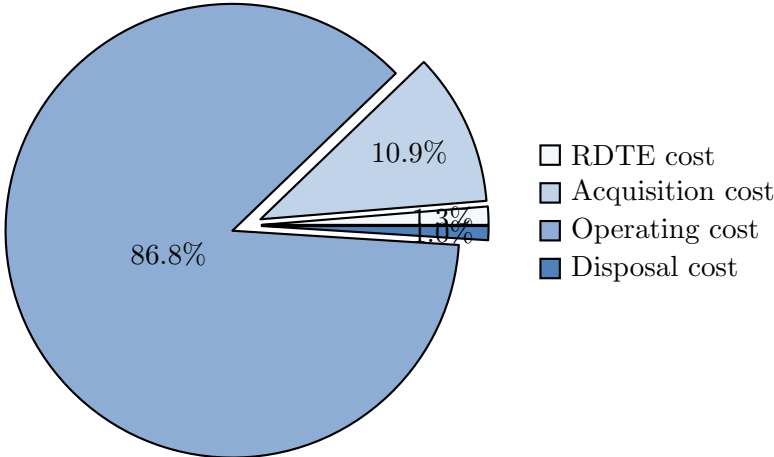
Figure 54: Contribution of items to the Life cycle cost

10 Structure and manufacturing

10.1 Systems

10.1.1 Fuel tanks and fuel pumps

Fuel system in FSB T-X aircraft is consisted of fuel tanks, fuel pumps and fuel lines, fuel venting system, fuel quantity indicating system, fuel management system, refueling system and system for simulation of air refueling. Since air-refueling will be simulated without actual fuel transfer, receiver mechanism for standard Air Force flying boom refueling is stowed and activated by pilot prior to air-refueling simulation. Most of the fuel is stored in wings, but because of insufficient storage space in wings and also requirement for the inverse flight there are also 2 fuel tanks placed in fuselage, as shown in picture (55).
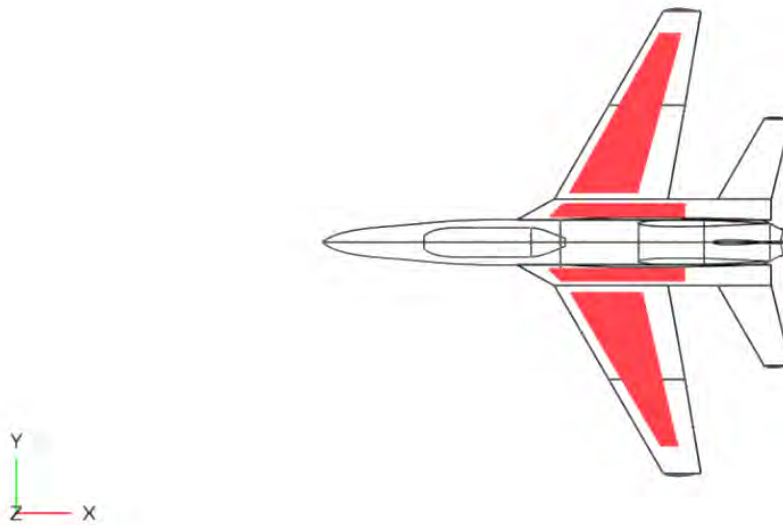
Figure 55: Fuel tank storage in the aircraft

10.1.2 Hydraulic system

Functions of hydraulic system are: moving flight controls and damping vibrations on them, extending and retracting of the landing gear, controlling wheel breaks, landing gear steering and operating thrust reversers. For executing those tasks hydraulic system is consisted of hydraulic fluid reservoir, hydraulic pumps, accumulators, lines and valves for fluid distribution, cockpit

controls to operate the functions served by the hydraulic system.

10.1.3 Electrical system

Electrical system provides electrical power for flight instrument and avionics system, internal and external lightning, engine starting systems and flight control systems. Electrical power is provided primary by engine driven generators and secondary by APU, RAT and batteries.

10.1.4 Environmental control system

Environmental control system is consisted of: pressurization system, pneumatic system, air-conditioning system and oxygen system. The purpose of these subsystems is to provide normal atmosphere conditions in cockpit while pneumatic system is also used as ice protection system.

10.1.5 System layout design

Pictures (56) and (57) show layout of main aircraft systems.
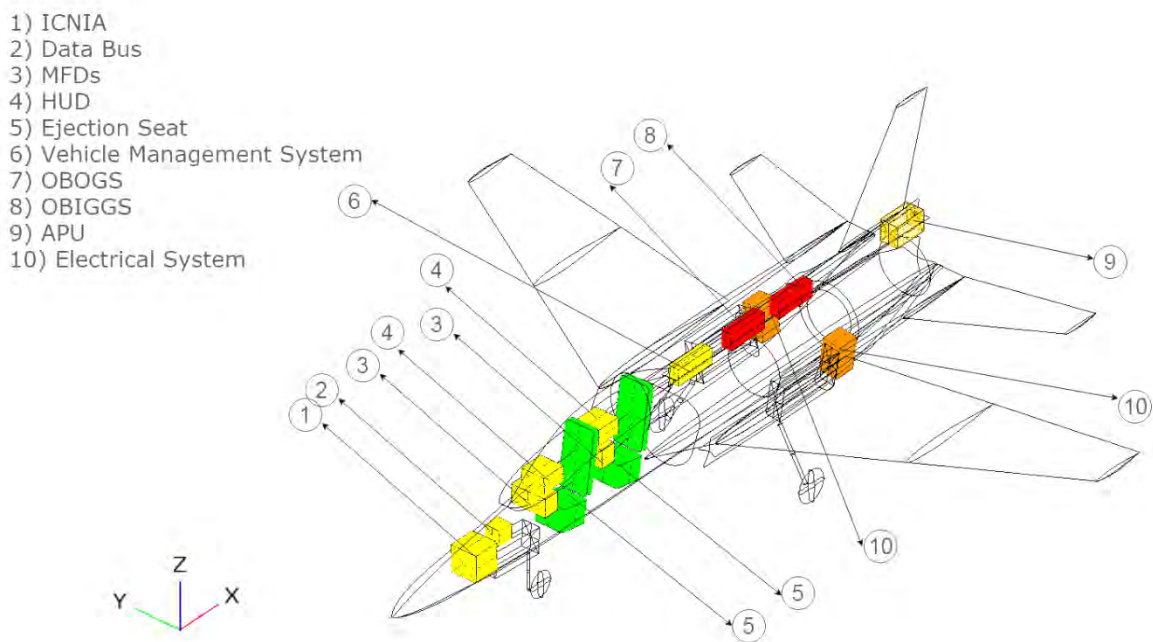
Figure 56: Layout of basic aircraft systems
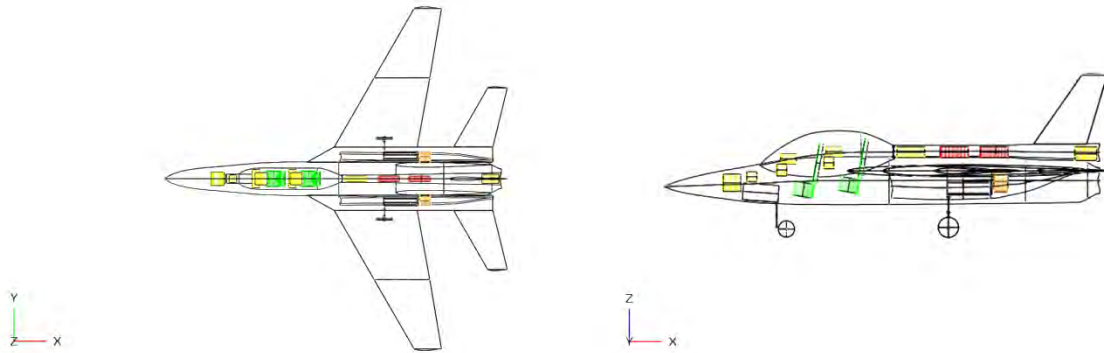
Figure 57: Top view and side view of basic aircraft systems

More detailed overview of the aircraft systems is given in figure (57). The list is based on aircraft systems used in 5 similar military and training aircrafts and default systems given by the RFP. Those aircrafts are F-22, F-16, KAI T-50 Golden Eagle, Aermacchi M-346 and Hawk T2. Due to aircraft safety, redundancy of system is used.

10.2   V-n diagram

In Table 17 are shown required data for V-n diagram.

Table 17: Required data for V-n diagram

Symbol	Name	Value
m	maximum gross weight	11023.1 lb
C_{lmax}	maximum positive lift coefficient	1.121 [-]
S	wing area	$177.6 ft^2$
b	span	29.79 ft
$n_{lim,pos}$	positive design limit load factor	9
$n_{lim,neg}$	negative design limit load factor	-3
$n_{ult,pos}$	positive ulitimate load factor	13.5
$n_{ult,neg}$	negative ulitimate load factor	-4.5

In Figure 58 are shown the V-n diagram, of the FSB-TX, which represents the aircraft load factor as a function of airspeed. Stall boundaries are shown in the diagram as well as positive

and negative design limit load factor and ultimate load factors. By observing the V-n diagram it is seen that the gust diagram shown in dashed lines does not influence the maneuver diagram. It is also relevant to note that the dive speed of 1.2 Ma (calculated from the maximum dynamic pressure of 2133 psf as given in the RFP) is higher than would be expected for the final design. According to [[3] [4] [5]] and a maximum cruise speed of 0.7 Ma would give this aircraft a dive speed of 0.875 Ma.
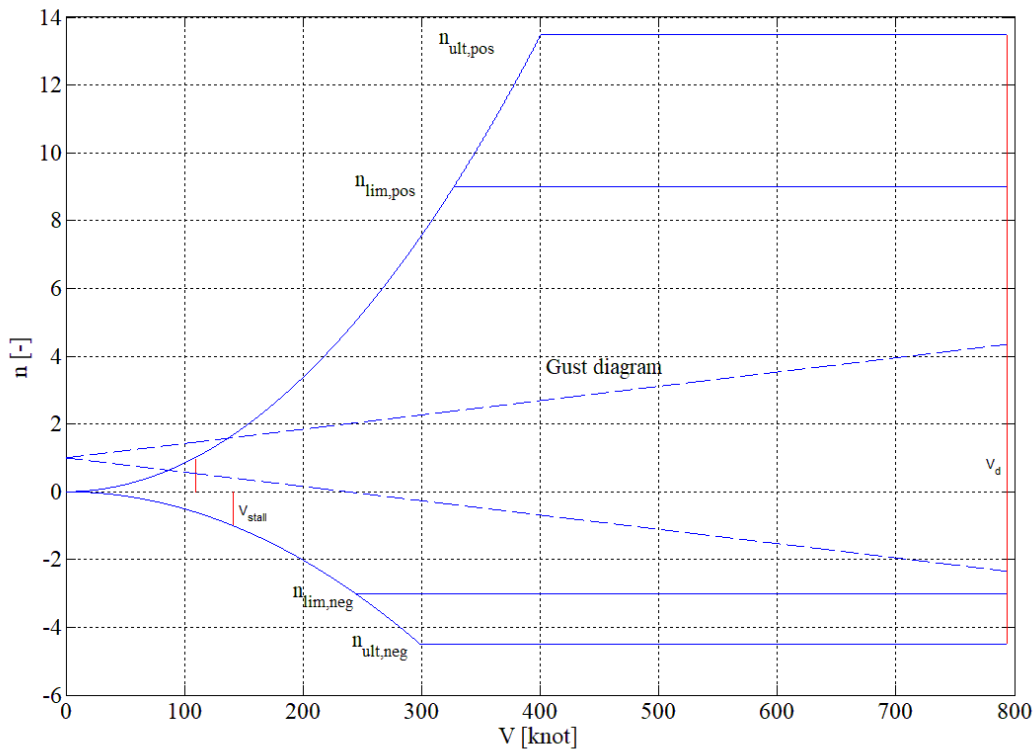
Figure 58: V-n diagram

10.3 Structural arrangement

The design of the training aircraft FSB T-X was made in accordance with the design of the Aermacchi M-346 training aircraft. The structural arrangement of fuselage, wing, and empennage are shown in figure 59 and 60. The fuselage of aircraft is made as the semi-monocoque structure composed of skin, frames, and longerons. The frames are replaced with pressure bulkheads on the entrance and exit of the cockpit. The mainframes are placed where fuselage and wings are attached and on the place where empennages and fuselage are attached. According

to the recommendation from Roskam [3] [4] [5], the mass reduction of the structure is made by using mainframes, who are already used for empennage, to mount engine. The mainframes who are used for attachment fuselage and wings are also used for attachment of the main landing gear, while the front landing gear is attached on pressure bulkhead. The wings and vertical tail surfaces are composed of ribs, spars, and skin. The horizontal tail surfaces (rudder) and other control surfaces are made of honeycomb composite material. The engine is attached in three points. Two points of attachment are placed on the mainframe behind wings, and the third point is placed on the mainframe where is attached front spar of the vertical tail surface. Attachment points are made of steel alloy.

Table 18: Wing components

Wing	SelectedSpacing / Location
Rib	10 inches
FrontSpar Location	15 %
MiddleSpar Spacing	15 - 19 inches
AftSpar Location	15 %

Table 19: Fuselage components

Fuselage	SelectedSpacing / Location
FrameSpacing	11 –20 inches
FrameDepth	2inches [3] [4] [5]
LongeronSpace	8 – 12inches [3] [4] [5]

Table 20: Vertical tail components

VerticalTail	SelectedSpacing / Location
RibSpacing	8 – 12inches
FrontSpar Locating	15 %
AftSpar Locating	75 %
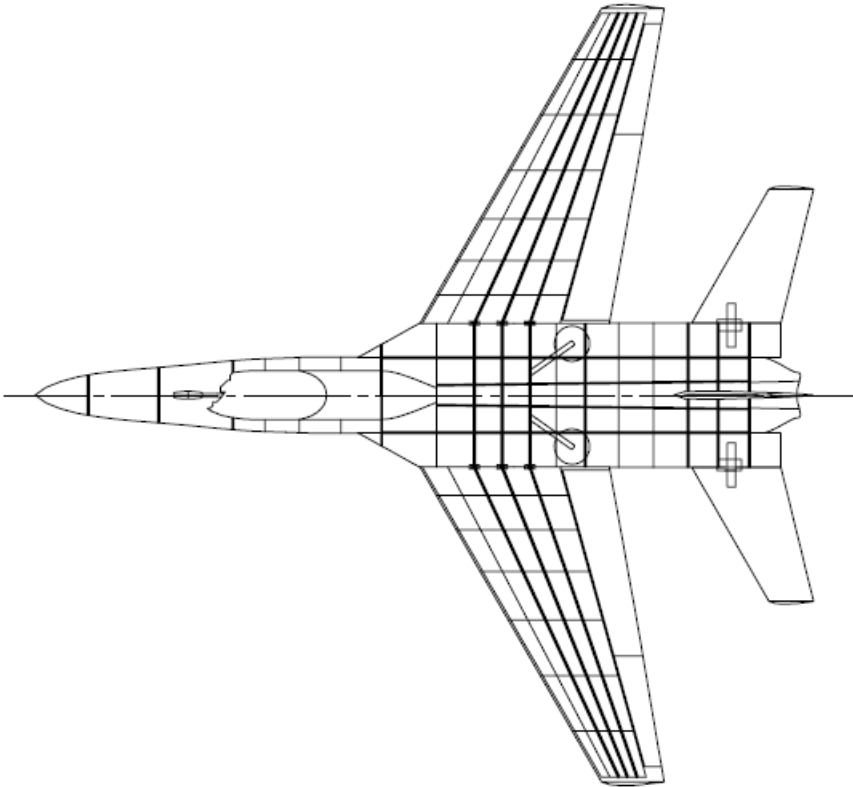
Figure 59: Top view of aircraft and structure elements
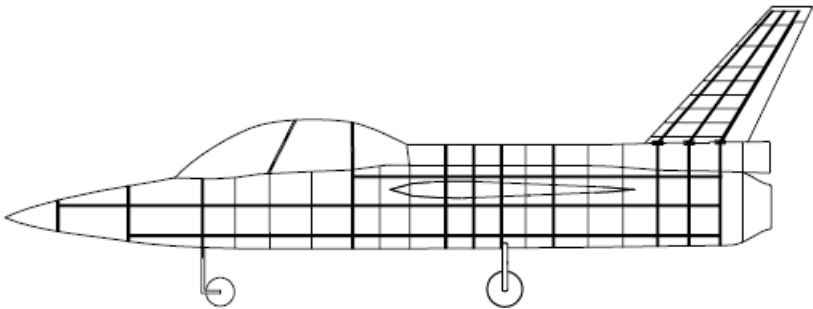
Figure 60: Side view of aircraft and structure elements

36.9220

14.1680

36.9980
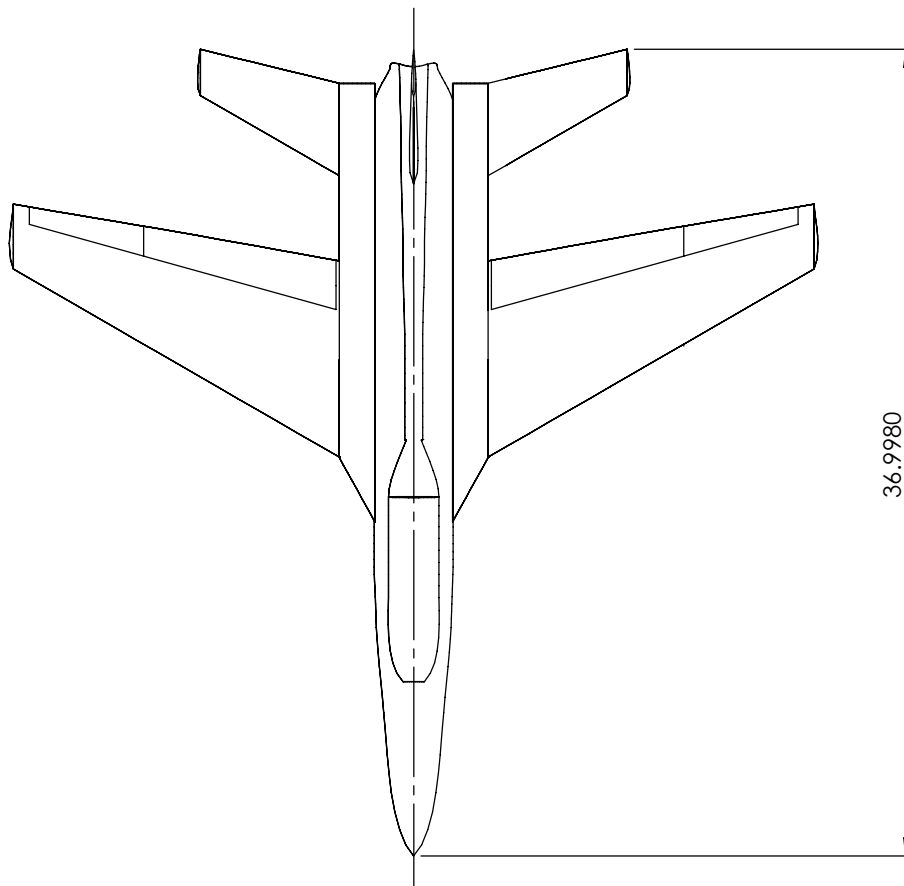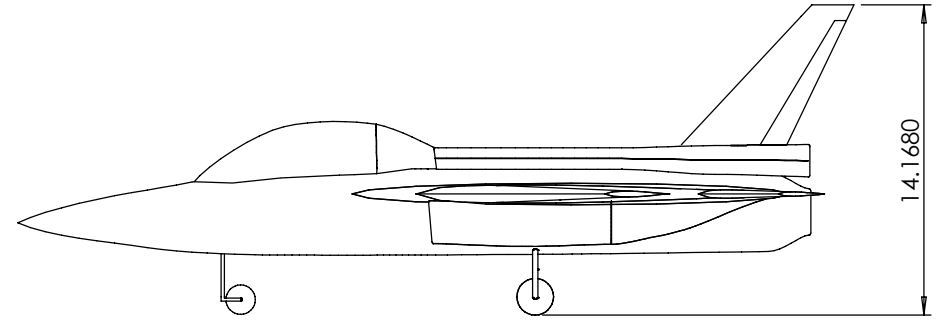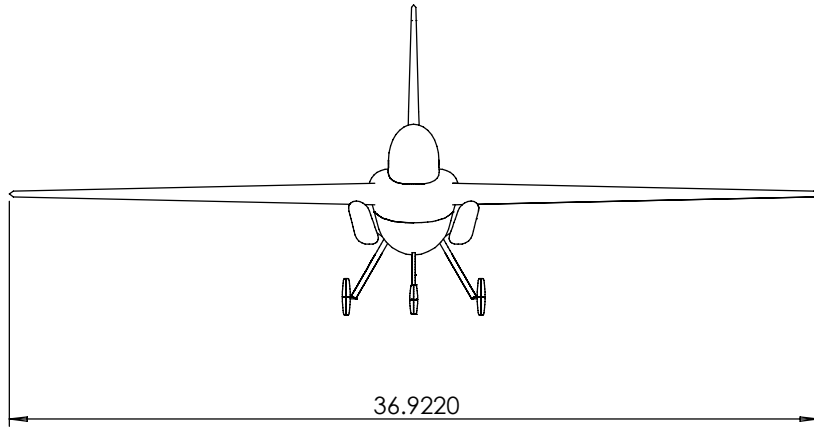
SCALE 1:100

	Wing	Horizontal Tail	Vertical Tail
Area - S	177 ft2	40.085 ft2	20.989 ft2
Span - b	29.80 ft	12.664 ft	6.061 ft
Root chord - cr	8.96 ft	4.222 ft	4.707 ft
Tip chord - ct	2.96 ft	2.110 ft	1.926 ft
Aerodynamic midchord - cA	6.46 ft	3.280 ft	3.576 ft
Aerodynamic apces - xA	4.20 ft	1.860 ft	1.430 ft
Incidence angle - i	0°	0°	0°
Dihedral angle - Γ	0°	0°	0°
Taper ratio - λ	0.33	0.5	0.4
Sweep angle - Λ 1/4	30°	30°	40°
Aspect ratio - AR	5	4	1.85
Inboard sweep- ΛLE	34.14°	-	-
Outbord sweep - ΛTE	15.38°	-	-
	Fuselage	Overall	
Length	36.209 ft	36.998 ft	
Maximal height	6.107 ft	14.168 ft	
Maximal width	6.824 ft	36.922 ft	

10.4   Material selection and technology

As a structural elements arrangement, materials for structural elements are selected according to training aircraft Aermacchi M-346. In Table 21 are given materials and manufacturing technology of structural parts.

Table 21: Materials and technologies for structural elements

Part	Material	Manufacturing Technology
Radomes	GFRP	autoclave
Windshield	acrylic/ polycarbonate	automated thermoforming
Pilot cabin cover	acrylic/ polycarbonate	automated thermoforming [6]
Canopy frame	Aluminium alloy - 7050	machining
Intake	Aluminium alloy - 7050	machining
Intake channel	CFRP	autoclave
Front fuselage skin	CFRP	autoclave
Middle fuselage skin	CFRP / Aluminium alloy - 5052	autoclave
Tail skin	CFRP / Aluminium alloy - 5052	autoclave [7]
Frames	Aluminium alloy 7075	machining
Fuselage and wing attachments	Aluminium alloy - 7175	machining
Wing skin	CFRP	autoclave
Leading edge and peaks	Aluminium alloy	machining + chemical treatment
Spars and ribs of wings	Aluminium alloy - 7050	machining

Ailerons and flaps	CFRP (skin) + aluminium honeycomb - 5052	autoclave , The thermal expansion, bonding
Horizontal tail	CFRP (skin) + aluminium honeycomb - 5052	autoclave , The thermal expansion, bonding
Fuselage and horizontal tail attachments	Aluminium alloy - 7050	machining
Skin of vertical tail	CFRP	autoclave
Spars and ribs of vertical tail	Aluminium alloy - 7050	machining
Fuselage and vertical tail attachments	Aluminium alloy - 7175	machining
Rudder	CFRP (skin) + aluminium honeycomb - 5052	autoclave , The thermal expansion, bonding
Landing gear	Steel alloy – AerMet 340 Alloy	minting
Pressure bulkhead	aluminium alloy 2124	machining
Engine mounts	steel chrome-molybdenum (4130)	machining

Table 21 shows that all basic structural elements are made of aluminum alloys and / or carbon fiber composite materials. More detailed information about the materials used in the individual structural elements are given as guidelines below.

- Radomes are made by E-glass fibers because of good radar permeability and significantly lower material price compared to other types of fibers. [[13]]

- The aluminum alloy is used for frames because of demands placed on them, such as strength, fatigue and damage resistance, and compression strength [14].

- The aluminum alloy 2124 will be used for pressure bulkheads [14].

- Airelons, flaps, rudder, and elevator are made of sandwich-structured composite made by honeycomb core and carbon fiber cover. Honeycomb core is made of aluminum alloy 5502 with a galvanic coating to protect aluminum from corrosion. The advantage of these

constructions is a relatively simple repair option (depending on the location of the damage) which has a beneficial effect on maintenance costs on the maintenance side.

• Due to its high strength requirements, the chassis is made of high strength steel with a low content of 300M alloy elements with a strength ranging from 1650 to 2000 MPa (240-290 ksi) [15].

It is important to emphasize that due to the reduction in production costs and thus the life cycle cost of the aircraft, all production technologies used to make the construction elements selected so that existing machines with possible minor modifications can be used.
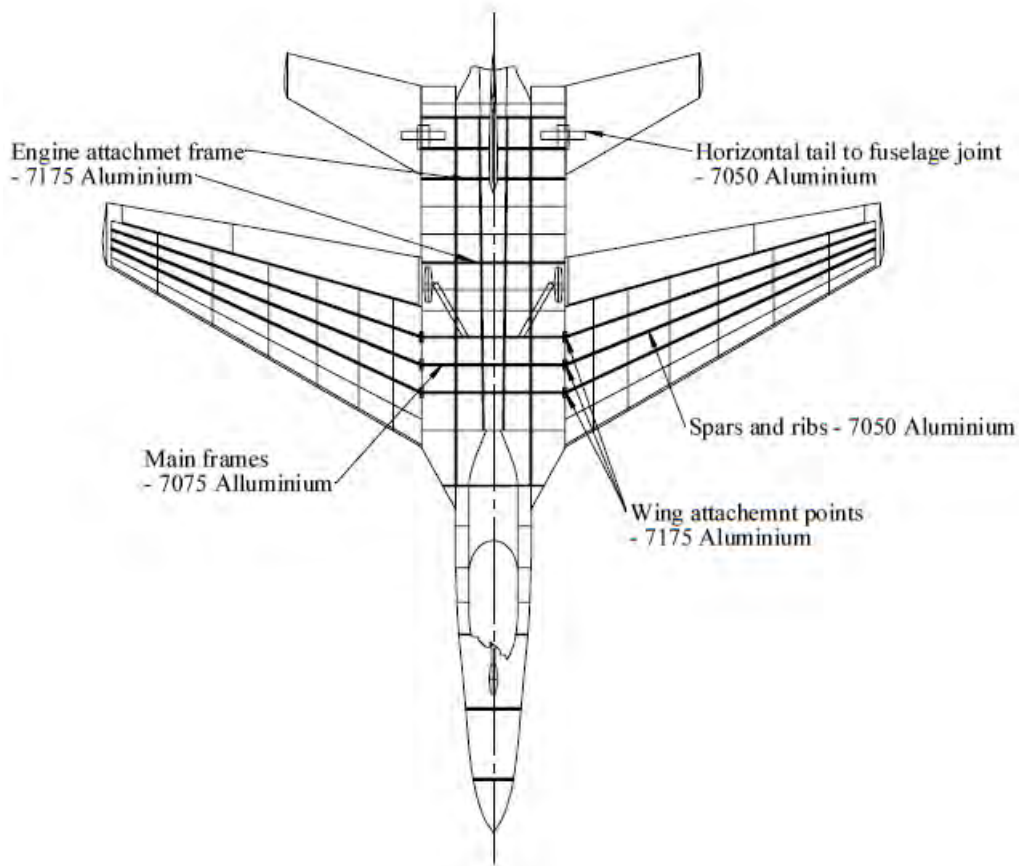
Figure 61: Aircraft parts and materials in the ground plan
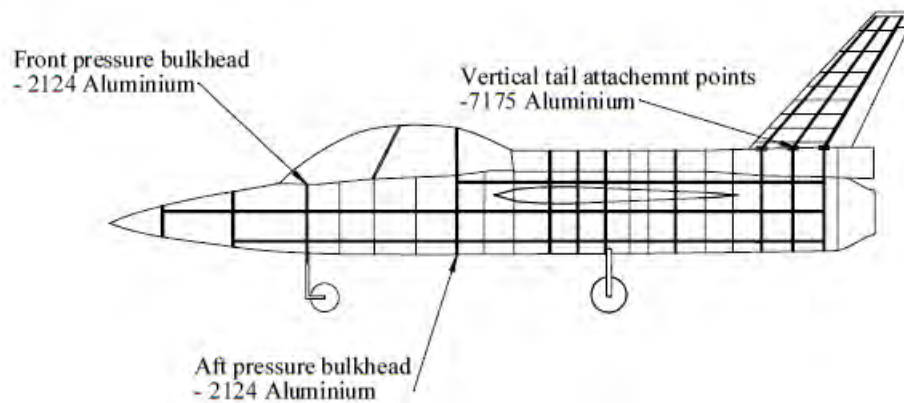
Figure 62: Parts and materials of the aircraft in the side view

10.5 Managment and Manufacturing

Aircraft production is divided into a stand-alone production of parts in the home facility and parts and equipment purchased as a finished product. As a finished product, all systems are built into the aircraft, the engine and the chassis. Aircraft production is divided into 4 production units:

1) Front of the fuselage (till the cockpit)

2) The middle part of the fuselage (from the rear pressure bar to the first stage of the compressor)

3) The rear of the fuselage with horizontal and vertical stabilizers

4) Wings

Each of the production units is subject to the following actions:

- production of appropriate structural elements

- assembly of structural elements

- installation of purchased parts

- final control

After completing all necessary operations on the production units, the final assembly is followed, where they are assembled into a finished product.

Each of the production units is subject to the following actions:

10.6   Maintenance

Since maintenance is one of the biggest contributions to the aircraft life cycle, it is important to optimize it as much as possible. Maintenance optimization for this aircraft was carried out through the following steps:

- Reducing the need and use of existing field equipment

- Opening the cockpit cover to the right for easier replacement of the pilot seats

- Setting all aircraft and electronics maintenance opening on the left at a level that does not require additional ground equipment (open down)

- One port through which all the fuel tanks in the level with the maintenance openings are also to the left

- Replacement of parts such as steering wheel, rudder height, actuators - lightweight parts procurement [16].

11   Conclusion

FSB-TX aircraft was designed in response to the 2017./2018. AIAA RFP for a new jet fighter training aircraft which was supposed to replace previously used T-38C Talon. Before the start of the design phase, it was necessary to determine a few main objectives which would later serve the team as guidelines and furthermore help in every decision that was made. After analysing a few jet fighter training aircraft, it was identified that the main difference between jet fighter training aircraft and all the other airplanes lays in the fact that the training airplanes have much more operating hours. The main drawback of having a large amount of operating hours is the frequency of maintenance operations which make the majority of overall airplane life cycle expenses. Because of that fact, it was commonly decided that the focus of this project should be on minimizing the life cycle cost. Since the airplane was meant to be designed for new pilots, the FSB-TX team found importance in enabling the pilot and the instructor to land safely almost everywhere in case of emergency, by minimizing the overall runway length. Afterwards, the team analysed the career path for the new pilots and decided that it would be the best to make the adaption process from the trainer aircraft to 5th generation fighters as easy as possible in terms of maneuverability. Having the main objectives in mind, the project could start with the weight estimation based on the information about the airplanes of similar purpose. When it came to the decision about the engine that will be used, a trade study was made. Five commercialy available jet engines were taken into consideration including F-404, F-414, F-110, Snecma M88 and Honeywell F125. Since all the combinations gave a similar value of take-off and empty weight, it was decided that the cheapest engine (Honeywell F125) should be the first candidate among all the engines previously taken into consideration. Before the final decision was made, performance estimation had to be made, so the team could be sure that the engine will satisfy all the requirements given by the RFP. Performance estimation showed that the engine that was chosen was found satisfactory although it had the lowest T/W ratio. Some more trade studies regarding the influence of the lift coeffiecient on take off, landing conditions and maneuvering were made to make a decision that would result with optimal wing construction regarding the price and performance. The wing was designed without slats to minimize the wing maintenance cost. As a consequence of the team striving to minimize the mass of every constructive element, vertical stabilizer was found to be too small for the lateral stability purpose which was detected on time and corrected by enlarging the vertical stabilizer construction. During the process of of

stability analysis, it was decided that the wing and tail configuration will be joined to the body in a way which will result with static instability in some regimes of the flight, so the airplane could be more maneuverable with the use of closed loop feedback system. All possible weight loading scenarios were taken into consideration in stability analysis to ensure that the static margin isn't larger than 13% of mean aerodynamic chord. The airplane was also tested against the MIL-F-8785-C by simulation which was done with *Ceasiom* and proved to be satisfactory, showing some good flying qualities. After the stability analysis, it was mandatory to check the performances one more time which resulted with final performance values that were found satisfactory in all cases. It was found that the design resulted with a very short runway length, even less than the value required by the RFP. Finally, the cost estimation was made, which resulted with pretty low prices compared to the competition. It can be concluded that the aircraft accomplished all the objectives that were set in the beginning of the project.

References

[1] Roskam J., *Airplane Design – Part I – Preliminary sizing of airplanes*. Roskam Aviation and Engineering Corporation. Kansas, 1985.

[2] Roskam J., *Airplane Design – Part II – Preliminary configuration desgin and integration of the propulsion system*.Roskam Aviation and Engineering Corporation. Ottawa, Kansas, 1985.

[3] Roskam J., *Airplane Design – Part III – Layout design of cockpit, fuselage, wing and empennage: cutaways and inboard profiles*. Roskam Aviation and Engineering Corporation. Ottawa, Kansas, 1986.

[4] Roskam J., *Airplane Design – Part IV – Layout design of landing gear and systems*. Roskam Aviation and Engineering Corporation. Ottawa, Kansas, 1986.

[5] Roskam J., *Airplane Design – Part V – Component weight estimation*. Roskam Aviation and Engineering Corporation. Ottawa, Kansas, 1985.

[6] Roskam J., *Airplane Design – Part VI – Preliminary calculation of aerodynamic, thrust and power characteristics*. Roskam Aviation and Engineering Corporation. Ottawa, Kansas, 1987.

[7] Roskam J., *Airplane Design – Part VII – Determination of stability, control and performance characteristics: FAR and Military requirements*. Roskam Aviation and Engineering Corporation. Ottawa, Kansas, 1988.

[8] Jankovic S. *Mehanika leta zrakoplova*. Poglavlje Kinematika leta. FSB. Zagreb, 2001.

[9] Jackson P. *Jane's All the World's Aircraft*. 2004-2005.

[10] Jackson P. *Jane's Aero Engines*. 2002

[11] `http://www.viscopedia.com/viscosity-tables/substances/aviation-fuels/` , *09.02.2018.*

[12] `http://airfoiltools.com/airfoil/details?airfoil=naca63209-il` , *09.02.2018.*

[13] Baker, A. , Dutton, S. , Kelly, D.: Composite Materials for Aircraft Structures , Second edition, AIAA 2004.

[14] N. Eswara Prasad, R. J. H. Wanhill.: Aerospace Materials and Material Technologies, Volume 1: Aerospace Materials, 2017.

[15] Niu, M.C.Y. ; Airframe Structural Design , 1988

[16] Maintenance Matters, https://www.boeing.com/features/2017/11/t-x-maintenance-matters.page , 16.04.2018.

[17] GKN Aerospace team win 2014 Defense Manufacturing Technology Award, http://www.adsadvance.co.uk/gkn-aerospace-team-win-2014-defense-manufacturing-technology-award.html , 25.04.2018.

[18] AIAA *Request for proposal – Advanced Pilot Training Aircraft.*

[19] Raymer D. *Aircraft Design: A Conceptual Approach.*

[20] *Jane's Aero Engines.*
    https://www.janes.com

[21] Jackson P. *Jane's All the World's aircraft 2004-2005.*

[22] Jackson P. *Jane's All the World's Aircraft.* 2004-2005.

[23] http://www.viscopedia.com/viscosity-tables/substances/aviation-fuels/ , *09.02.2018.*

[24] https://airfoiltools.com/airfoil/details?airfoil=n0009sm-il , *27.03.2018.*

[25] Jackson P. *Jane's All the World's Aircraft.* 2004-2005.

[26] Jackson P. *Jane's Aero Engines.* 2002

[27] Abbott, Ira Herbert, and Albert Edward Von Doenhoff. *Theory of wing sections, including a summary of airfoil data.* Courier Corporation, 1959.